2014

The Effects of Sea Surface Temperature Gradients on Surface Turbulent Fluxes

John Steffen

FLORIDA STATE UNIVERSITY

COLLEGE OF ARTS AND SCIENCES

THE EFFECTS OF SEA SURFACE TEMPERATURE GRADIENTS ON SURFACE TURBULENT FLUXES

By

JOHN STEFFEN

A Thesis submitted to the
Department of Earth, Ocean, and Atmospheric Science
in partial fulfillment of the
requirements for the degree of
Master of Science

Degree Awarded:
Summer Semester, 2014

John Steffen defended this thesis on June 18, 2014.
The members of the supervisory committee were:

Mark A. Bourassa
Professor Directing Thesis

Robert Hart
Committee Member

Jeffrey Chagnon
Committee Member

The Graduate School has verified and approved the above-named committee members, and certifies that the thesis has been approved in accordance with university requirements.

ACKNOWLEDGMENTS

This work has been supported by NASA Climate Data Records and the NASA Ocean Vector Winds Science Team. I would like to thank my major professor, Dr. Mark Bourassa, and my committee members (Dr. Hart and Dr. Chagnon) for their guidance and support throughout this research project.

TABLE OF CONTENTS

LIST OF TABLES

LIST OF FIGURES

ABSTRACT

A positive correlation between sea surface temperature (SST) and wind stress perturbation near strong SST gradients (ΔSST) has been observed in different parts of the world ocean, such as the Gulf Stream in the North Atlantic and the Kuroshio Extension east of Japan. These changes in winds and SSTs can modify near-surface stability, surface stress, and latent and sensible heat fluxes. In general, these small scale processes are poorly modeled in Numerical Weather Prediction (NWP) and climate models. Failure to account for these air-sea interactions produces inaccurate values of turbulent fluxes, and therefore a misrepresentation of the energy, moisture, and momentum budgets. Our goal is to determine the change in these surface turbulent fluxes due to overlooking the correlated variability in winds, SSTs, and related variables.

To model these air-sea interactions, a flux model was forced with and without SST-induced changes to the surface wind fields. The SST modification to the wind fields is based on a baroclinic argument as implemented by the University of Washington Planetary Boundary-Layer (UWPBL) model. Other input parameters include 2-m air temperature, 2-m dew point temperature, surface pressure (all from ERA-interim), and Reynolds Daily Optimum Interpolation Sea Surface Temperature (OISST).

Flux model runs are performed every 6 hours starting in December 2002 and ending in November 2003. From these model outputs, seasonal, monthly, and daily means of the difference between ΔSST and no ΔSST effects on sensible heat flux (SHF), latent heat flux (LHF), and surface stress are calculated. Since the greatest impacts occur during the winter season, six additional December-January-February (DJF) seasons were analyzed for 1987–1990 and 1999–2002.

The greatest differences in surface turbulent fluxes are concentrated near strong SST fronts associated with the Gulf Stream and Kuroshio Extension. On average, 2002–2003 DJF seasonal differences in SHF, LHF, and wind stress over the Gulf Stream are 3.86 ± 0.096 W/m², 6.84 ± 0.186 W/m², and 0.032 ± 0.0008 N/m², respectively. In addition, smaller flux differences covering large expanses of the Atlantic and Pacific Oceans are non-negligible for most upper oceanic applications sensitive to multi-decadal changes. Due to these non-linear processes, average changes in surface turbulent fluxes are not zero.

CHAPTER ONE

INTRODUCTION

Modification of surface winds within the Marine Atmospheric Boundary Layer (MABL) by large sea surface temperature gradients (ΔSSTs) has been observed and modeled in different parts of the world ocean [Chelton, 2005; Chelton et al., 2007; O'Neill et al., 2010; Small et al., 2008; Song et al., 2006]. However, the effects that air-sea coupled processes near SST gradients have on surface turbulent heat fluxes are largely unaccounted for in weather and climate models. The goal of this study is to determine how large of a difference in surface turbulent fluxes of momentum, sensible heat, and latent heat occurs due to overlooking the correlated variability in SSTs, winds, and temperatures over the Gulf Stream and Kuroshio Extension.

SST gradients on the order of ~100-200 km are associated with western boundary currents, such as the Gulf Stream (North Atlantic) and the Kuroshio Extension (North Pacific). A positive correlation exists between SSTs and wind stress in these regions, suggestive of the ocean forcing the atmosphere [Small et al., 2008]. Contrarily, on larger scales, across entire ocean basins, the correlation is often negative. Positive wind speed perturbations cool the ocean surface through evaporation and may increase the entrainment of cool upper-thermocline waters into the mixed layer, indicating that the atmosphere is driving an oceanic response [Small et al., 2008]. Therefore, complex interactions in air-sea coupling near strong SST gradients are likely responsible for the positive correlation observed at smaller spatial scales.

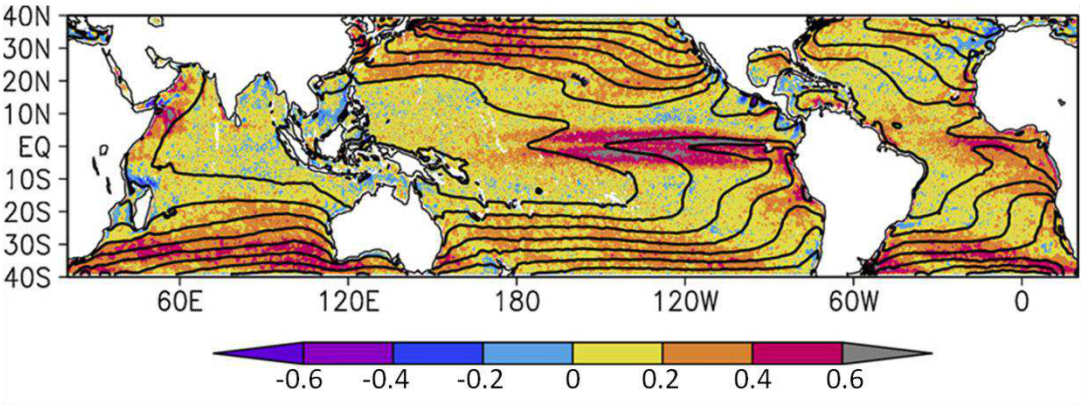

Figure 1.1: Correlation (color) between SST and neutral 10m wind speed from TRMM TMI data for 1997-2004 (pre-filtered to emphasize mesoscale features). The annual-mean SST is overlaid in black contours (interval of 2°C, ranging from 14°C to 30°C) [Small et al., 2008].

The following relationships between SST and wind stress (Fig. 1.2) are consistently observed from satellite observations in the vicinity of strong SST gradients [Chelton et al., 2001, 2004, 2007; O'Neill et al., 2003, 2005]:

- Perturbations in wind stress magnitudes are linearly related to perturbations in SST
- Perturbations in wind stress divergence are linearly related to the downwind SST gradient (perpendicular to SST isotherms)
- Perturbations in wind stress curl are linearly related to the crosswind SST gradient (parallel to SST isotherms)

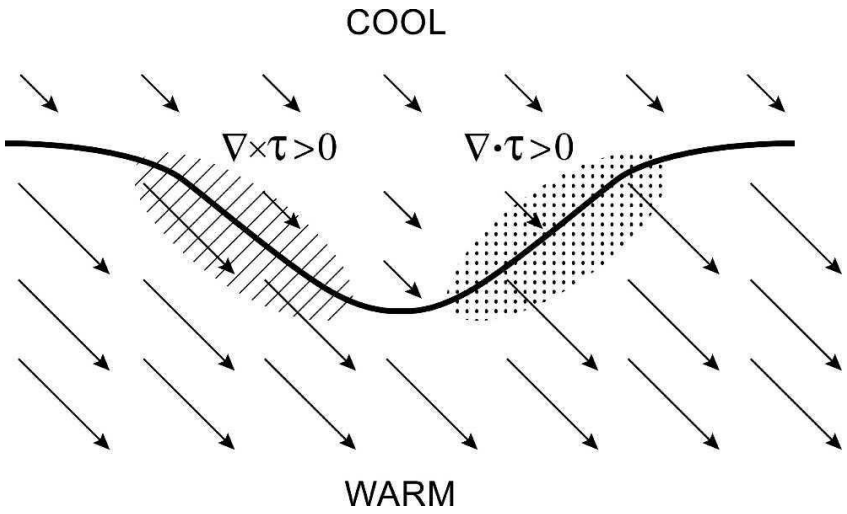

Figure 1.2: Schematic showing SST gradient influences on surface winds. Wind stress magnitudes (represented by the lengths of the vectors) are stronger on the warm side of the SST front and weaker on the cold side, leading to enhanced regions of wind stress curl (hatched) and divergence (stippled) [Chelton et al., 2007].

The effects of SST gradients on surface winds and turbulent heat fluxes influence the ocean and atmosphere over a wide range of spatial and temporal scales. These large turbulent heat fluxes play an important role in mesoscale and synoptic-scale atmospheric processes, such as coastal frontogenesis, the formation of coastal low-level jets, the generation of low-level clouds and rainbands, and the intensification of midlatitude frontal systems [Xue et al., 2000]. On larger spatial and temporal scales, diabatic heating resulting from surface heat fluxes over the Gulf Stream and North Atlantic Ocean is fundamental for maintaining climatological atmospheric circulations in the region and over Europe [Minobe et al., 2008]. In addition, ocean

modeling studies suggest that Ekman upwelling near strong SST gradients has a significant effect on local and large-scale ocean circulations [Milliff et al., 2004]. All of these coupled air-sea processes contribute to the substantial impact that large SST gradients have on the ocean and atmosphere.

To model these impacts (Chapter 2), two surface wind data sets were created using the University of Washington Planetary Boundary Layer (UWPBL) model; a control data set that lacks SST gradient influences and a perturbed data set that applies a baroclinically-driven modification to the surface winds [Paul Hughes, personal communication, 2013]; this modification is called the thermal wind term in the UWPBL documentation [J. Patoux, UWPBL 4.0, 2004]. To quantify the response of surface turbulent fluxes to the air-sea coupling that occurs near strong SST gradients, a flux model [Bourassa, 2006] was forced with both surface wind data sets, separately (Chapter 2.3). Then, differences in sensible heat flux (SHF), latent heat flux (LHF), and wind stress were determined by subtracting the control run from the experimental run. Seasonally averaged results from the December 2002 through November 2003 calendar year show a seasonal cycle in surface turbulent flux differences (Chapter 3). The greatest impacts over the Gulf Stream and Kuroshio Extension occur during the winter, while a minimum is reached over the summer. Since the largest differences in surface turbulent fluxes occur during the winter, six additional December-January-February (DJF) seasons from 1987-1990 and 1999-2002 were analyzed (Chapter 3.2.1). Slight differences in the histogram distributions can be attributed to interannual variability in large scale atmospheric circulations.

Overall, surface turbulent flux differences during the winter season can be substantial for a wide range of atmospheric and oceanic applications. Even small turbulent flux differences in the summer months can impact upper ocean heat content on multi-decadal time scales [Levitus et al., 2005]. These findings indicated that a more detailed representation of the air-sea coupled processes near SST gradients would improve the moisture, energy, and momentum budgets in climate models and gridded reanalyses.

1.1 Background

There are two main physical mechanisms related to momentum mixing that explain increased surface winds over warm SSTs and suppressed surface winds over cool SSTs: a stability-related mechanism and a pressure gradient perturbation mechanism (Fig. 1.3).

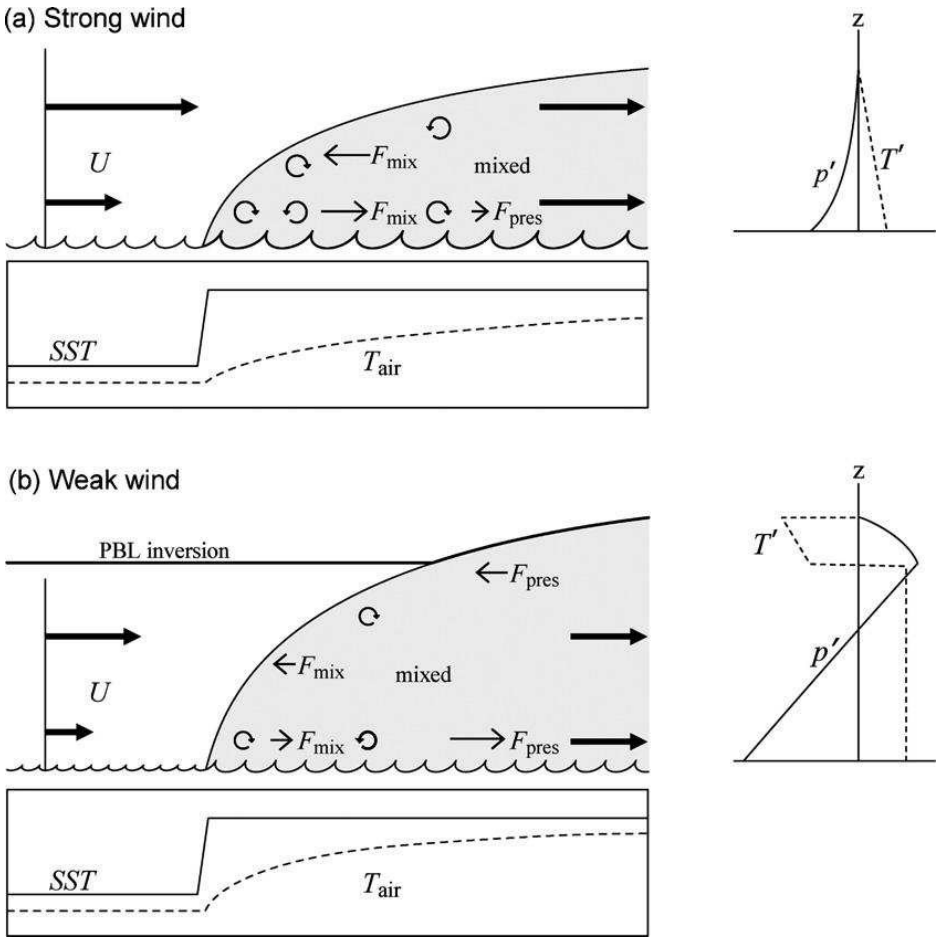

Figure 1.3: Schematic showing the boundary layer response to a SST front. The surface winds (bold arrows) are from cold to warm SST for conditions with (a) strong background winds and (b) weak background winds. A mixed internal boundary layer (gray shading) develops downstream with circular arrows indicating enhanced turbulent mixing. Forces due to mixing and pressure are indicated with thin arrows. Below each panel are horizontal across-front profiles of SST and air temperature. To the right of each panel are the vertical profiles of the downstream air temperature anomalies (dashed) and pressure anomalies (solid) [Small et al., 2008].

The stability mechanism uses a near-surface stability argument to describe the positive correlation between surface winds and SSTs [Wallace et al., 1989]. As surface winds blow across an SST gradient, air-sea temperature and humidity differences are generated leading to changes in near-surface stability. The near-surface logarithmic profiles are modified such that the vertical gradients of wind speed, air potential temperature and humidity are increased in stable conditions and decreased in unstable conditions [Chelton et al., 2001]. Stable conditions develop as relatively warm boundary layer air from the warm side of the SST front is advected over cooler SSTs, effectively decoupling the surface winds from the winds aloft. Due to the stable

stratification within the boundary layer, downward turbulent mixing of momentum is inhibited and surface winds decelerate. Unstable conditions are generated as relatively cool and dry continental air masses are advected over the warm side of the SST front. Stronger winds higher up in the MABL are more efficiently mixed downwards, accelerating the surface winds. Additionally, the development of a pressure gradient perturbation across the SST front [Lindzen and Nigam, 1987] produces a positive correlation between surface winds and SSTs. As winds blow across an SST gradient, the MABL adjusts to the underlying SSTs. Higher pressure and descending air over the colder water and lower pressure and ascending air over the warmer water force a thermally direct circulation within the MABL that accelerates the surface winds from colder to warmer water [O'Neill et al., 2005].

The dynamic and thermodynamic response of surface winds to SST gradients is not entirely understood, since both physical mechanisms likely contribute to the positive correlation. For example, strong winds crossing a sharp SST gradient do not have time to adjust to the underlying SSTs and therefore the stability mechanism is dominant. Conversely, during weak surface winds, the air temperature has time to reach equilibrium with SSTs, and the pressure gradient mechanism dominates. Thus, the different physical mechanisms that adjust surface winds in the presence of SST gradients operate in different regions and are influenced by the magnitude of the SST gradient and the direction of the large scale winds [Hogg et al., 2009]. However, analyzing differences between satellite and buoy observations, stability played only a small role in the Gulf Stream region [O'Neill, 2012]. Regardless of the physical mechanism, the adjustment of surface winds by SST gradients has been conclusively observed in satellite and in situ data.

Major western boundary ocean currents, such as the Gulf Stream and the Kuroshio Extension play an important climatic role by transporting warm subtropical water poleward, resulting in large transfers of sensible and latent heat from the ocean to the atmosphere [Song et al., 2009]. Winter-time climatological latent and sensible heat fluxes from the Gulf Stream and Kuroshio currents to the atmosphere are on the order of 200-300 W/m² and 50-100 W/m², respectively. Summer-time heat fluxes are smaller but still substantial, with magnitudes of 50-100 W/m² and -15 to 15 W/m² [Josey et al., 1999]. The changes in surface turbulent heat fluxes associated with surface wind speed perturbations over strong SST gradients are likely to be underestimated in modeled gridded data with grid spacing of 1° or more [Rouault et al., 2003].

The ability of climate models to simulate air-sea interactions over western boundary currents degrades with decreasing horizontal and vertical grid resolution [Maloney and Chelton, 2006].

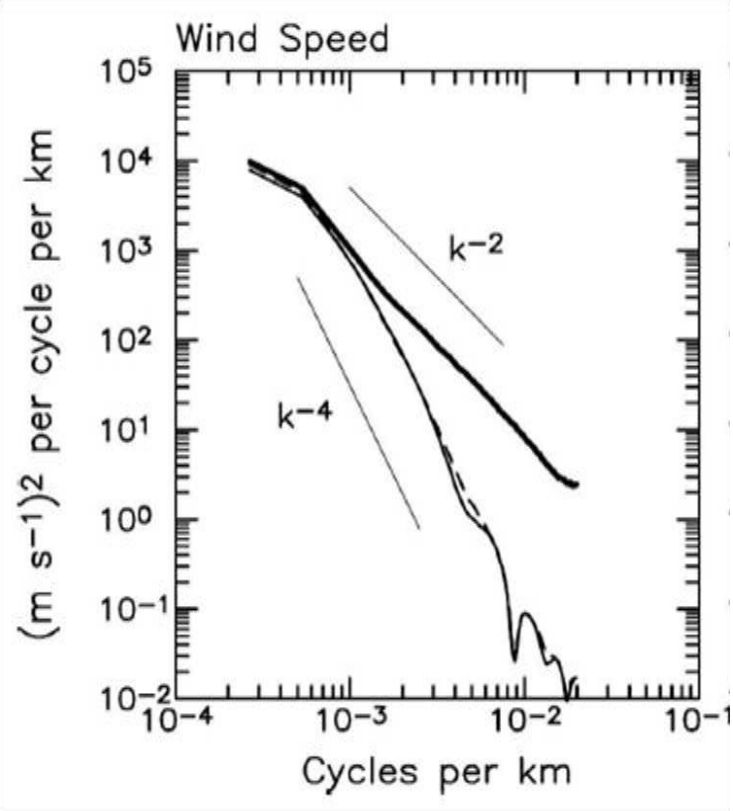

Figure 1.4: Along-track wavenumber spectra of 10m wind speed in the eastern North Pacific Ocean for 2004 computed from QuikSCAT observations (heavy solid line), NCEP analyses (thin solid line), and ECMWF analyses (dashed lines) [Chelton et al., 2006].

Winds in NWP models and reanalysis data sets have considerably less energy at spatial scales smaller than ~1000 km (Fig. 1.4). This result can be seen in the wavenumber spectra of 10m wind speeds from observations during the Tropical Ocean Global Atmosphere Coupled Ocean-Atmosphere Response Experiment (TOGA COARE) and from satellite-based observations when compared to National Centers for Environmental Prediction (NCEP) and European Centre for Medium-Range Weather Forecasts (ECMWF) reanalyses [Wikle et al., 1999; Milliff et al. 2004; Chelton et al. 2006]. Therefore, significant errors in the energy and moisture budgets likely exist in climate models and reanalysis data sets due to their inability to effectively resolve the air-sea interactions that occur across SST fronts.

CHAPTER TWO

METHODS

To model air-sea interactions near strong SST fronts, a flux model based on Monin-Obukhov similarity theory [Bourassa, 2006; Zheng et al., 2013] was forced with two sets of data: one that adjusted surface winds in response to small scale SST gradients and one that lacked this small scale coupling (Fig. 2.1). Both sets of fields were produced with surface pressures, air temperatures, and humidities from the ERA-Interim product [Dee et al., 2011] and Reynolds Daily Optimum Interpolation (OI) SST [Reynolds et al., 2007]. The control six-hourly wind fields were created using the above information as input into the University of Washington Planetary Boundary Layer (UWPBL) model. The control case was initiated without including surface wind variability due to baroclinicity or boundary-layer stratification. In our experimental case, SST gradients are used as a proxy for air temperature gradients and the underlying SST is communicated to the near-surface air temperature. This introduces baroclinicity into the system and modifies surface winds due to pressure-related changes within the boundary layer. On the spatial scale of approximately 25 km considered in this analysis, wind speed and SST coupling are dominated by this baroclinic variability and are qualitatively and quantitatively consistent with the vast majority of observations mentioned in the introduction [Paul Hughes, personal communication, 2013].

In addition, the UWPBL is numerically unstable for large deviations from neutral stability. Since stratification is presumed to play an important role in surface turbulent fluxes, the neutral stability UWPBL fluxes were not used. Instead, we calculate stability-dependent fluxes by forcing a flux model with the two surface wind data sets produced by the UWPBL model and additional surface variables from ERA-Interim (Fig. 2.1). In summary, the only difference in bulk variables from the control case is the baroclinic change to the surface wind vectors in the experimental case. These bulk variables are then used to determine stability-dependent fluxes. Finally, surface turbulent flux differences of momentum, sensible heat, and latent heat are calculated by subtracting the control case from the experimental case.

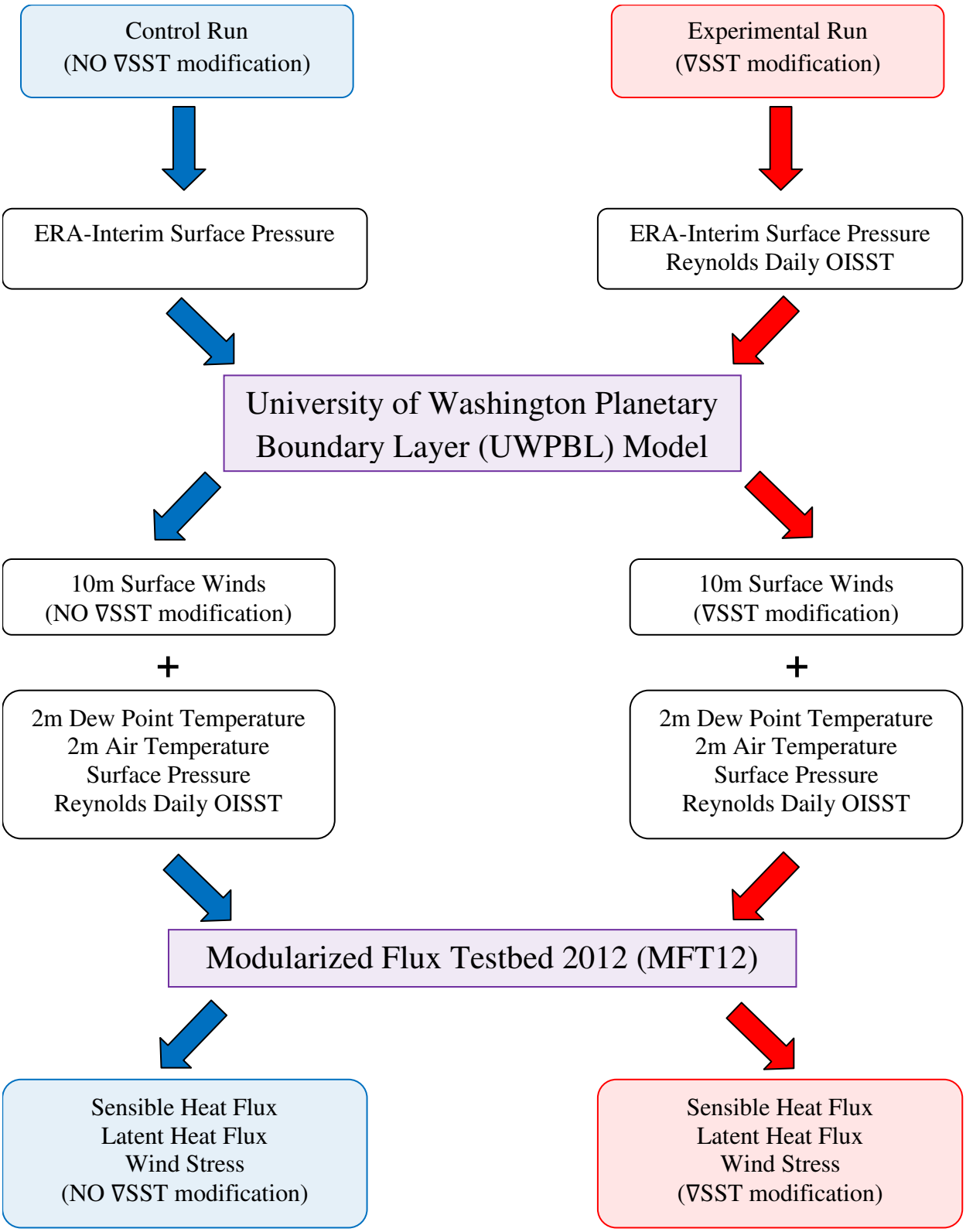

Figure 2.1: Flow chart describing the process of creating the control and experimental 10m surface wind data sets from the UWPBL model and how stability-dependent surface turbulent fluxes were calculated from the MFT12 flux model.

2.1 The UWPBL model and surface wind modification

The UWPBL is a modified atmospheric Ekman layer model for the midlatitudes implemented in direct form. Given the geostrophic wind, the direct model calculates the surface wind speed, turning angle, and other PBL characteristics [J. Patoux, UWPBL 4.0, 2004]. Geostrophic winds are computed from ERA-interim surface pressure fields. Stratification, baroclinicity, and secondary flows can be accounted for within the model provided they are small perturbations from a neutral case and are not too far from barotropic (SST gradients are capped at 2.2K per 100 km). For the midlatitudes, a modified Ekman spiral layer is patched to a near-surface logarithmic layer to construct the wind profile throughout the entire boundary layer. Matching conditions at the patch height between the Ekman layer and the logarithmic layer are based upon simple relationships between the surface stress and the geostrophic flow [Brown, 1974, 1978; Brown and Liu 1982]. The surface wind modifications were made for the December-January-February (DJF) seasons from 1987 – 1990 and 1999 – 2002, and also for the entire year from December 2002 through November 2003.

2.2 Reynolds Daily OI with microwave SSTs

The Reynolds OISST analyses blend in situ data from ships and buoys with satellite SST observations from the Advanced Very High Resolution Radiometer (AVHRR) and the Advanced Microwave Scanning Radiometer (AMSR) to produce a daily SST product with 0.25° grid spacing. The SST analyses are constructed using an optimum interpolation (OI) method [Reynolds et al., 2007] that utilizes error correlation length scales of approximately 900 km zonally and 600 km meridionally. The selection of large length scales avoids sampling errors due to the sparse distribution of in situ observations and limited infrared satellite observations from cloud contamination [Song et al., 2009]. As a result, spatial scales less than 1000 km are poorly resolved by Reynolds SST analyses, leading to a significant underestimation of the SST gradients on the spatial scales associated with western boundary currents such as the Gulf Stream and Kuroshio Extension. In fact, the small-scale SST gradient magnitudes computed from the Reynolds SST analyses are about a factor of 5 smaller than those computed from the AMSR SST data [O'Neill et al., 2005]. As an example, the sharp SST front of the Kuroshio Extension supports SST gradients as large as 10°C over 100 km [Nonaka and Xie, 2003]. In this study, the SST gradient magnitudes are limited to a maximum of 2.2 K/100 km to ensure the stability of the

UWPBL model. For these reasons, forcing the UWPBL model with Reynolds Daily OI SST analyses represents a lower bound on surface wind modifications due to air-sea coupled processes near strong SST gradients. As a result, differences in surface turbulent heat fluxes and wind stress are conservatively estimated since these variables are related to surface wind speeds.

2.3 MFT12 flux model description

A practical approach to modeling surface turbulent fluxes is to utilize a bulk flux model and conventional meteorological variables from the MABL. The Modularized Flux Testbed 2012 (MFT12) allows users to combine a variety of parameterizations related to air-sea interaction to compute surface turbulent fluxes and height adjustments for wind, temperature, and humidity.

Molecular diffusion is the primary process that transfers water vapor at the air-sea interface. Mass transfer rates are determined by surface renewal theory, in which small fluid parcels near the air-sea interface are constantly exchanged with new elements from above, based on the residence time distribution of the surface elements. Therefore, turbulence within the interfacial sublayer can be parameterized using a surface renewal timescale [Clayson et al., 1996].

For this study, the Bourassa [2006] surface roughness model, which includes the effects of capillary waves and sea state, was used with the Clayson, Fairall, and Curry (CFC) roughness length parameterization [Clayson et al., 1996] for potential temperature and moisture and the Zheng et al. [2013] transition from a smooth to rough surface. Additionally, Benoit's [1977] parameterization for an unstable boundary layer and the Beljaars and Holtslag [1991] stable boundary layer parameterization are applied. The Monin-Obukhov scale length is calculated as described by Liu et al. [1979]. These parameterizations implement Monin-Obukhov similarity theory with a surface renewal model in order to accurately determine surface turbulent fluxes. The vertical fluxes of momentum (τ), heat (H), and moisture (E) are defined in terms of the friction velocity (u_*), and the analogous terms for potential temperature and moisture (θ_* and q_*, respectively):

$$\vec{\tau} = \rho \vec{u}_* |u_*|$$
$$H = -C_p \rho \theta_* |u_*|$$
$$E = -L_v \rho q_* |u_*|$$

where ρ is the air density, C_p is the heat capacity of air, and L_v is the latent heat of vaporization [Bourassa et al., 1999]. The directional sign convention for wind stress is positive downward and for energy fluxes is positive upward.

The domain ranges from 115.125°E to 25.125°E and 20.125°N to 75.125°N, encompassing most of the northern Pacific and Atlantic Oceans and, most importantly, the Gulf Stream and Kuroshio Extension ocean currents. Point-by-point calculations of sensible heat flux, latent heat flux, and wind stress are calculated with 0.25° grid spacing and a six-hourly temporal resolution.

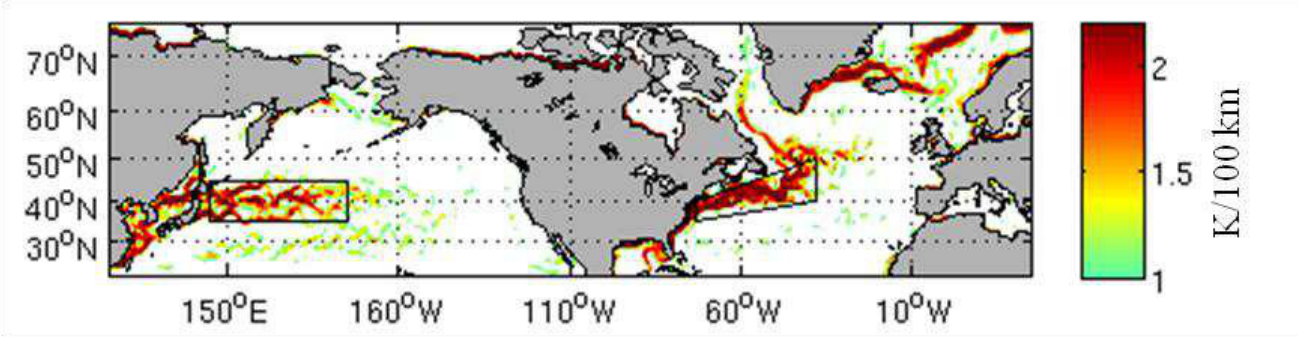

Figure 2.2: 2002 – 2003 DJF seasonal averages of SST gradients greater than 1K/100 km covering the entire domain. The trapezoids enclose the locations of strongest SST gradients over the Gulf Stream and Kuroshio Extension.

The MFT12 flux model ingests a suite of atmospheric and oceanographic parameters. Non-constant variable fields for equivalent-neutral (EN) wind speed, surface pressure, 2-m dew point temperature, 2-m air temperature, and SST are model inputs. The fields for surface pressure, 2-m dew point temperature, and 2-m air temperature are obtained from the ERA-Interim reanalysis dataset. A 2-D spline interpolation is used to regrid the ERA-Interim variable fields to match the equivalent-neutral 10-m wind speed fields derived from the UWPBL model. Also, SST skin temperatures are approximated as the Reynolds Daily OI SST values. This assumption is poor in areas of very low wind speeds (< 2 m/s) which are subject to large departures due to diurnal heating. The coupling of diurnal heating and baroclinic induced wind changes is beyond the scope of this work. In addition, there are several assumed physical constants used in the flux calculations (Table 2.1).

Table 2.1: Constant input parameters for MFT12 flux model

Parameter	Value	Units
Convective parameter	0.6	None
Surface moisture	98% RH	Fraction
Salinity	0.0349	Fraction

2.4 Surface turbulent fluxes

The flux model calculates values for sensible heat flux, latent heat flux, and wind stress for both the control and experimental model runs. The only difference between these two model runs is the ∇SST-induced modification of the surface winds in the experimental run. Therefore, any changes in surface turbulent heat fluxes are a direct result of the surface wind speed modifications by the UWPBL model due to the inclusion of ∇SST-induced baroclinic effects. Differences in the heat fluxes and wind stresses were calculated within the polygon regions (Figs. 3.1 and 3.2) encompassing the Gulf Stream and Kuroshio Extension by subtracting the control run values from the experimental run and averaging over daily, monthly, and seasonal time scales. From these mean differences, an examination of the histograms and box-and-whisker plots reveals a seasonal cycle in the turbulent heat fluxes and the expected result of increased variability at shorter time scales. The magnitude and location of turbulent heat flux differences across varying spatial and temporal scales has wide-ranging impacts. From climatological to frontogenesis scales, these ∇SST-induced changes in turbulent heat fluxes can have an impact on the energy and moisture budgets.

CHAPTER THREE

RESULTS

Point-by-point calculations of surface turbulent fluxes of momentum, sensible heat, and latent heat were produced at 6 hour intervals for the entire year from December 2002 through November 2003. Since the largest surface turbulent flux differences tend to occur in winter, six additional DJF seasons were analyzed from 1987 – 1990 and 1999 – 2002. These years were chosen due to data availability. Flux differences were averaged over seasonal, monthly, and daily time scales to determine the magnitude and location of the largest surface flux differences.

A vast majority of the domain is not characterized by large SST gradients and therefore lacks the enhanced small-scale variability in surface winds associated with the air-sea coupling discussed. For this reason, surface turbulent flux differences are mainly concentrated near the large SST gradients associated with western boundary surface currents. To analyze these differences, the MFT12 flux model outputs were subset into two polygon regions: one enclosing the Gulf Stream and the other, the Kuroshio Extension. From the data subsets, histograms and box-and-whisker plots highlight the seasonal cycle in surface turbulent flux differences and provide insight into their magnitudes.

3.1 SST gradients and surface wind differences

The SST gradients computed from the Reynolds Daily OISST data for the Gulf Stream and Kuroshio Extension are similar in terms of magnitude and location across all seasons. The subset regions (Figs. 3.1 and 3.2) encompass the largest SST gradients where surface wind speed modifications are maximized. On seasonal time scales, especially for DJF, wind speed differences approach 1.0 m/s and cover much of the domain. The surface wind speed differences peak during winter, enter a transitional period in the spring and fall seasons, and reach a minimum during the summer. This annual cycle likely results from seasonal changes in the large-scale wind direction and surface wind speed that are consistent with the seasonal progression of the mean large-scale sea level pressure field [O'Neill, 2012]. Strong offshore winds blow from cooler to warmer SSTs during the winter months, creating unstable surface conditions and enhanced surface turbulent heat fluxes. Contrarily, winds are much weaker during the summer months and generally blow along the Gulf Stream or with a weak cross-isotherm

component from warmer to cooler SSTs, generating stable surface conditions [O'Neill, 2012]. Therefore, the large-scale seasonal wind characteristics impact the magnitude of the surface wind speed modifications and the associated turbulent heat flux differences.

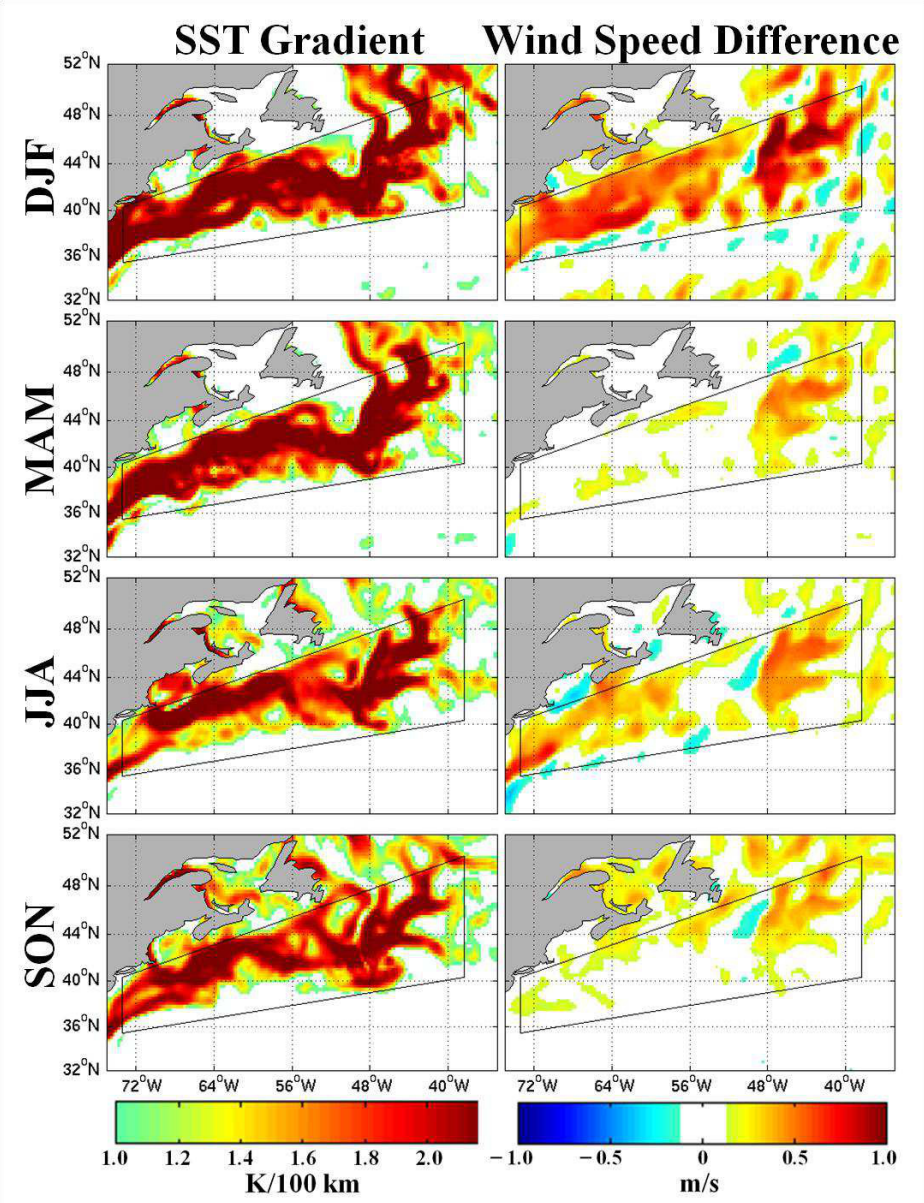

Figure 3.1: Seasonal averages of SST gradients (K/100 km) and wind speed differences (m/s) over the Gulf Stream for DJF (top row), MAM (2nd row), JJA (3rd row), and SON (bottom row). The trapezoids enclose the locations of strongest ∇SST-induced perturbations to the surface winds and turbulent heat fluxes.

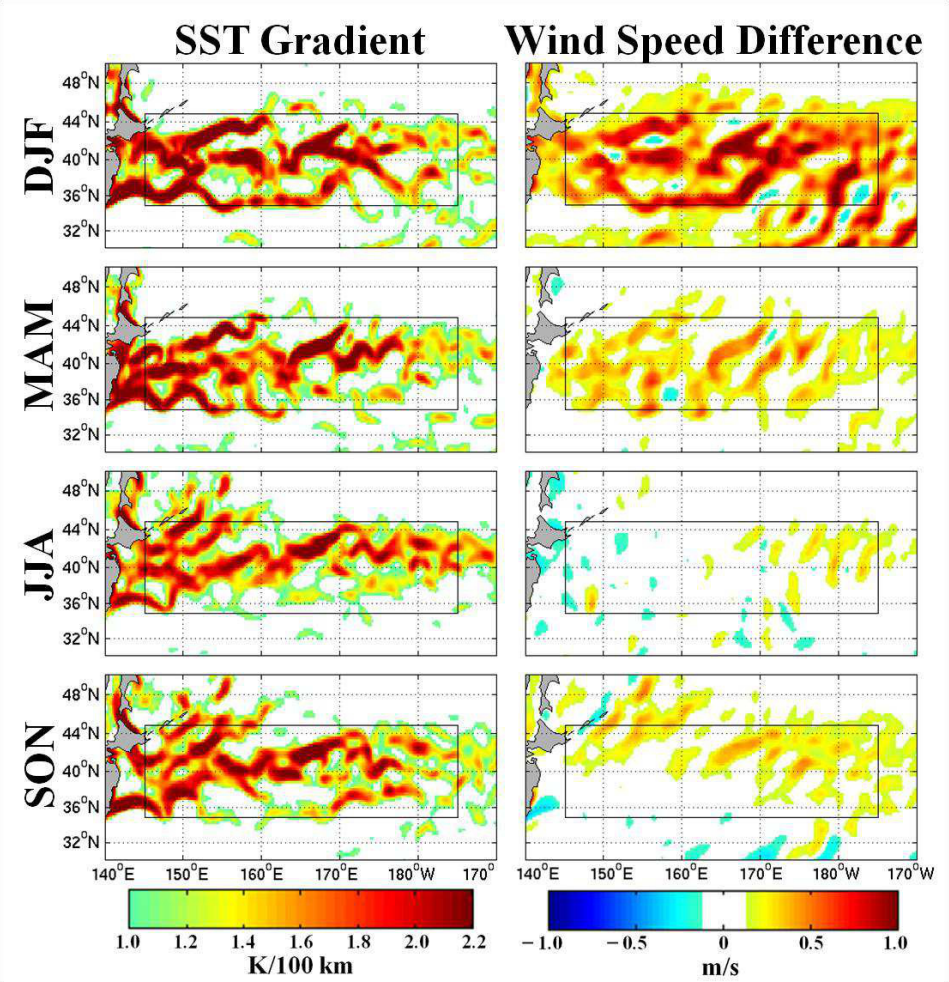

Figure 3.2: Seasonal averages of SST gradients (K/100 km) and wind speed differences (m/s) over the Kuroshio Extension for DJF (top row), MAM (2nd row), JJA (3rd row), and SON (bottom row). The trapezoids enclose the locations of strongest ∇SST-induced perturbations to the surface winds and turbulent heat fluxes.

3.2 Seasonal turbulent flux differences

Differences in surface turbulent fluxes exhibit a seasonal cycle as values peak during winter (DJF), subside through spring (MAM), reach a minimum in summer (JJA), and build back in fall (SON). As a result, the DJF season is particularly important when discussing the impacts these differences have on a variety of scientific applications spanning many spatial and temporal scales. Large expanses of ocean near the Gulf Stream and Kuroshio Extension have DJF seasonal heat flux differences over 5 W/m², with a small fraction surpassing 20 W/m² (Fig. 3.3). Wind stress differences are also at a maximum, reaching magnitudes of ~ 0.1 N/m². As the DJF season transitions to MAM, there is a substantial reduction in the surface turbulent flux differences. For

sensible and latent heat, the areas covered by large differences are substantially reduced and magnitudes are mostly under 5 W/m² (Fig. 3.3). Likewise, wind stress differences are mainly limited to less than 0.05 N/m² in MAM. During summer, these heat flux differences reach a minimum over the Gulf Stream and Kuroshio Extension, rarely surpassing 2 W/m² (Fig. 3.3). Interestingly, the largest flux differences for JJA occur off the U.S. west coast and the Baja peninsula of Mexico as the prevailing surface winds shift and interact with the California Current System (CCS) [Chelton et al., 2007]. While the sensible heat flux difference is minimal, a large area along the coast has latent heat flux differences approaching 5 W/m² and wind stress differences between 0.05 and 0.10 N/m² (Fig. 3.3). Finally, surface flux differences over the Gulf Stream and Kuroshio Extension begin to rebound in SON and have very similar magnitudes as MAM (Fig. 3.3).

The DJF winter season histograms have broader distributions than other seasons and peaks that are shifted toward positive differences as more extreme wind events tend to occur during the winter season resulting in greater turbulent flux differences (Fig. 3.4). This result is also seen in the box-and-whisker plots for the Gulf Stream (Fig. 3.5), with the largest DJF seasonally averaged differences in sensible heat, latent heat, and wind stress reaching 3.86 ± 0.096 W/m², 6.84 ± 0.186 W/m², and 0.032 ± 0.0008 N/m², respectively (Table 3.1). DJF seasonal flux differences over the Kuroshio Extension exhibit similar magnitudes of 3.76 ± 0.071 W/m², 7.37 ± 0.138 W/m², and 0.036 ± 0.0007 N/m², respectively (Table 3.2). The uncertainty in these mean differences is expressed as approximately ± two standard deviations. The two transitional seasons, MAM and SON, see a substantial reduction in magnitudes by a factor of approximately three when compared to DJF. The histogram shapes for MAM and SON fall in between the extremes of DJF and JJA. In general, the MAM and SON distributions have a shorter central peak than JJA and are positively skewed like DJF. Contrarily, the JJA summer season histograms have high, sharp peaks centered near zero difference (Fig. 3.4), representing very little variance from zero in the flux differences. As a result, JJA seasonal mean flux differences are negligible over the Gulf Stream and Kuroshio Extension for almost all upper oceanic applications on temporal scales smaller than multi-decadal changes, which are sensitive to several tenths of 1 W/m² [Levitus et al., 2005].

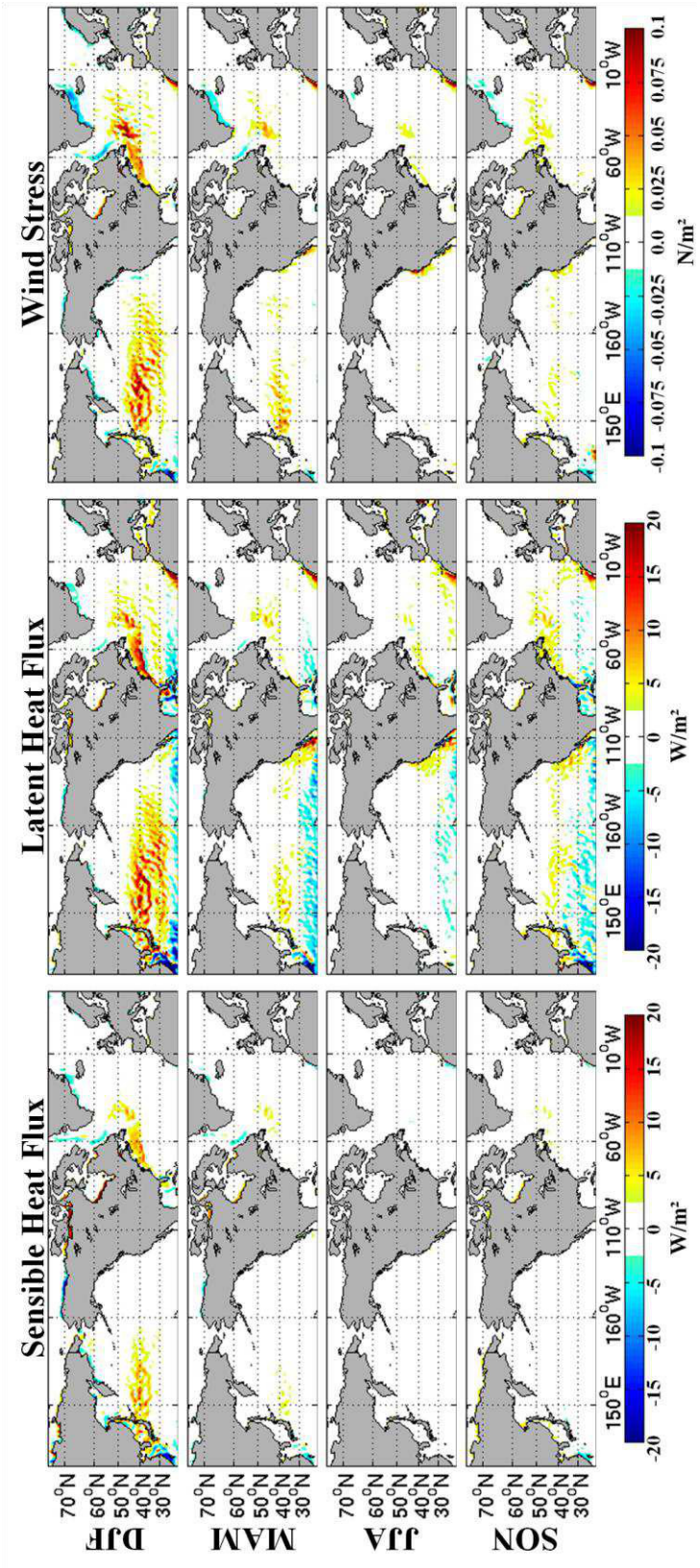

Figure 3.3: 2002–2003 seasonal average differences in SHF (left), LHF (middle), and wind stress (right) for DJF (top row), MAM (2nd row), JJA (3rd row), and SON (bottom row).

Table 3.1: Seasonally averaged differences in surface turbulent fluxes of momentum, sensible heat, and latent heat over the Gulf Stream.

Sensible Heat Flux [W/m²]	**Mean**	**95% CI**	**Standard Deviation**	**Range**
DJF	3.86	± 0.096	3.14	-2.91/12.48
MAM	0.89	± 0.042	1.37	-2.49/7.50
JJA	-0.05	± 0.021	0.67	-2.92/2.35
SON	1.07	± 0.030	0.98	-2.27/4.10
Latent Heat Flux [W/m²]	**Mean**	**95% CI**	**Standard Deviation**	**Range**
DJF	6.84	± 0.186	6.05	-7.35/27.43
MAM	1.63	± 0.061	2.00	-2.58/11.50
JJA	1.34	± 0.057	1.86	-3.65/11.32
SON	2.56	± 0.073	2.39	-4.91/9.79
Wind Stress [10^{-2} N/m²]	**Mean**	**95% CI**	**Standard Deviation**	**Range**
DJF	3.19	± 0.082	2.68	-2.56/11.30
MAM	0.89	± 0.036	1.17	-1.00/5.38
JJA	0.66	± 0.021	0.70	-0.88/2.60
SON	0.69	± 0.027	0.88	-1.18/4.74

Table 3.2: Seasonally averaged differences in surface turbulent fluxes of momentum, sensible heat, and latent heat over the Kuroshio Extension.

Sensible Heat Flux [W/m²]	**Mean**	**95% CI**	**Standard Deviation**	**Range**
DJF	3.76	± 0.071	2.89	-4.45/13.26
MAM	0.85	± 0.026	1.06	-1.98/5.62
JJA	0.02	± 0.008	0.32	-1.26/1.27
SON	0.34	± 0.017	0.70	-2.84/2.55
Latent Heat Flux [W/m²]	**Mean**	**95% CI**	**Standard Deviation**	**Range**
DJF	7.37	± 0.138	5.59	-4.94/26.76
MAM	2.11	± 0.047	1.89	-2.74/12.69
JJA	-0.02	± 0.017	0.70	-2.11/2.41
SON	1.43	± 0.051	2.08	-7.78/7.22
Wind Stress [10^{-2} N/m²]	**Mean**	**95% CI**	**Standard Deviation**	**Range**
DJF	3.62	± 0.065	2.64	-2.01/11.51
MAM	1.45	± 0.035	1.44	-1.92/6.32
JJA	0.06	± 0.008	0.33	-0.64/1.69
SON	0.54	± 0.016	0.63	-0.90/2.64

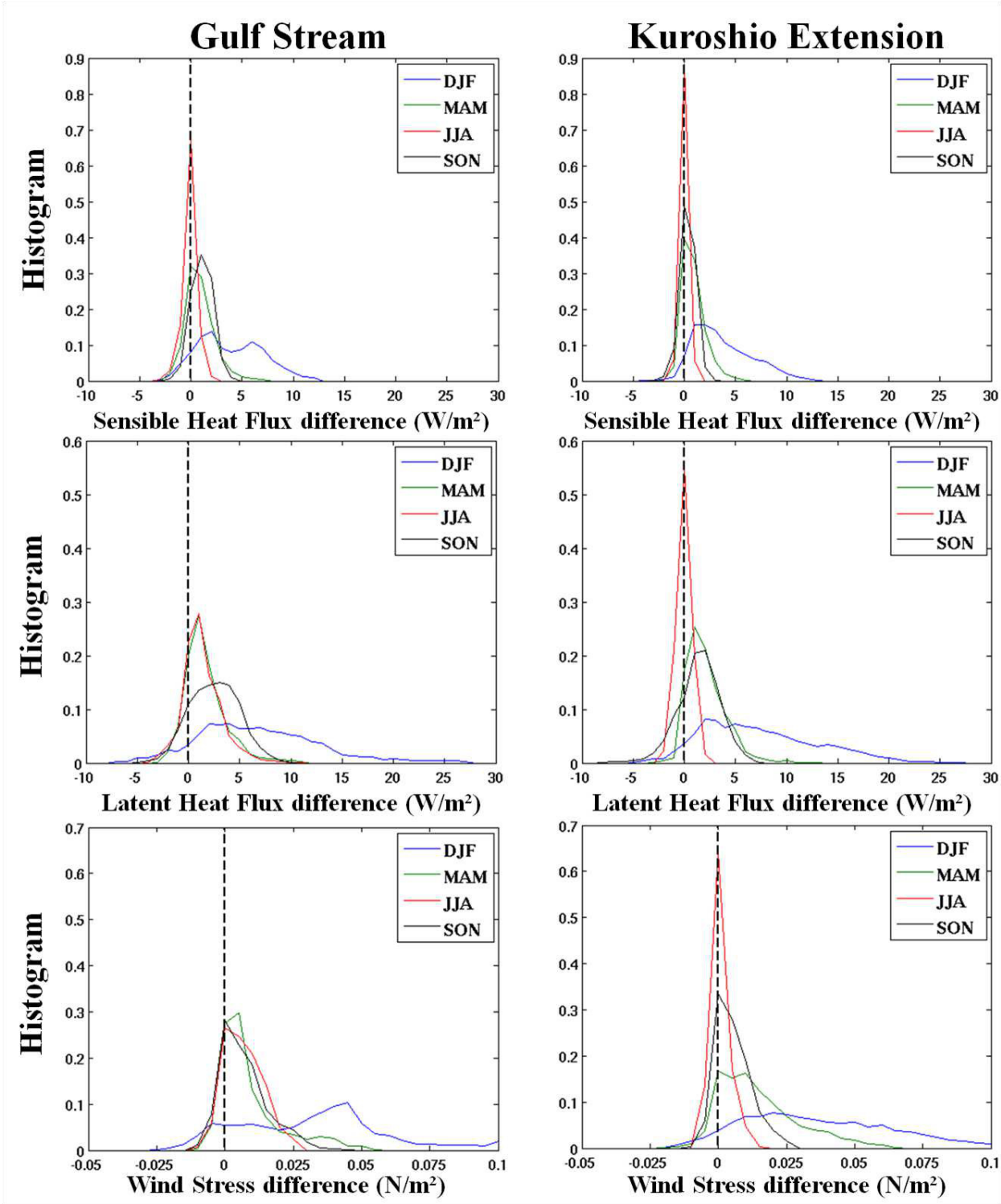

Figure 3.4: 2002–2003 seasonal histograms of SHF difference (top), LHF difference (middle), and wind stress difference (bottom) over the Gulf Stream (left) and Kuroshio Extension (right).

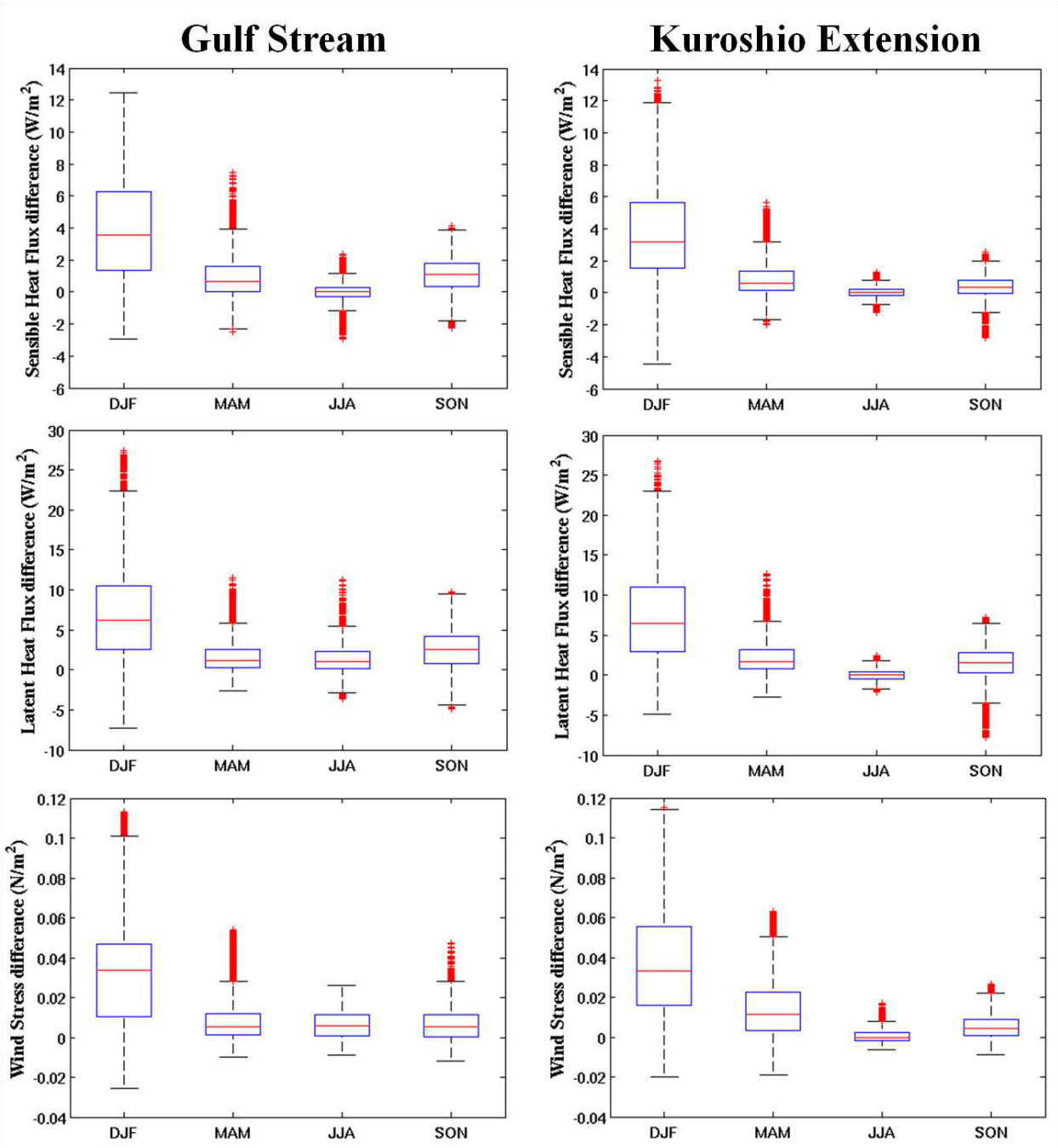

Figure 3.5: 2002–2003 seasonal box-and-whisker plots of SHF difference (top), LHF difference (middle), and wind stress difference (bottom) over the Gulf Stream (left) and Kuroshio Extension (right). The central mark is the median, the upper and lower edges of the box are the 75th and 25th percentiles, the whiskers extend to the most extreme data points, and the outliers are plotted individually.

3.2.1 Additional DJF seasons

The response of surface turbulent fluxes to ∇SST-induced modification of surface winds near the Gulf Stream and Kuroshio Extension is concentrated during the DJF winter season as a more active synoptic-scale environment and strong near-surface instabilities drive these air-sea coupled processes. To further study these coupled air-sea effects, additional DJF seasons were analyzed (Fig. 3.6) for 1987–1988, 1988–1989, 1989–1990, 1999–2000, 2000–2001, and 2001–2002. There is remarkable consistency in the magnitudes of flux differences amongst the six DJF seasons over the Kuroshio Extension and more variability in the flux differences over the Gulf Stream (Fig. 3.6). This is likely a result of physical differences between the Gulf Stream and Kuroshio Extension regions that influence the strength of the coupling between SST gradients and surface winds.

The histograms for sensible heat flux, latent heat flux, and wind stress differences tend to have broad distributions with slightly positive skewness. Since more extreme wind events and larger near-surface instabilities tend to occur during DJF, the positive tails of the distributions have more weight and large turbulent flux differences are more common than in other seasons (Fig. 3.6). As expected, most of the Gulf Stream histograms are unimodal with a central peak that is shifted toward positive differences. Interestingly, there are a few exceptions where the distributions are bimodal; these examples have a primary peak centered near 1 to 2 W/m² difference and a secondary peak centered near 6 to 7 W/m² difference. One example that stands out is the SHF difference over the Gulf Stream for the 2002–2003 DJF season that shows a distinct bimodal distribution. However, none of the Gulf Stream SHF differences for the other DJF seasons exhibit this bimodality. Additionally, most of the Gulf Stream wind stress differences are bimodal as well, with one peak centered near zero difference and a larger peak between 0.025 and 0.05 N/m². This is a result for the Gulf Stream distributions that is not observed in the Kuroshio Extension wind stress difference histograms (Fig. 3.6). The large dissimilarities between the wind stress difference histograms over the Gulf Stream and Kuroshio Extension are likely a manifestation of physical differences between the two regions. Factors such as the ∇SST magnitudes, near-surface stability, and the directional orientation of ∇SST differ between the two regions and may contribute to the differences seen in the turbulent flux histograms. A more detailed review of these regional differences and their implications is provided in the discussions section (Chapter 3.5).

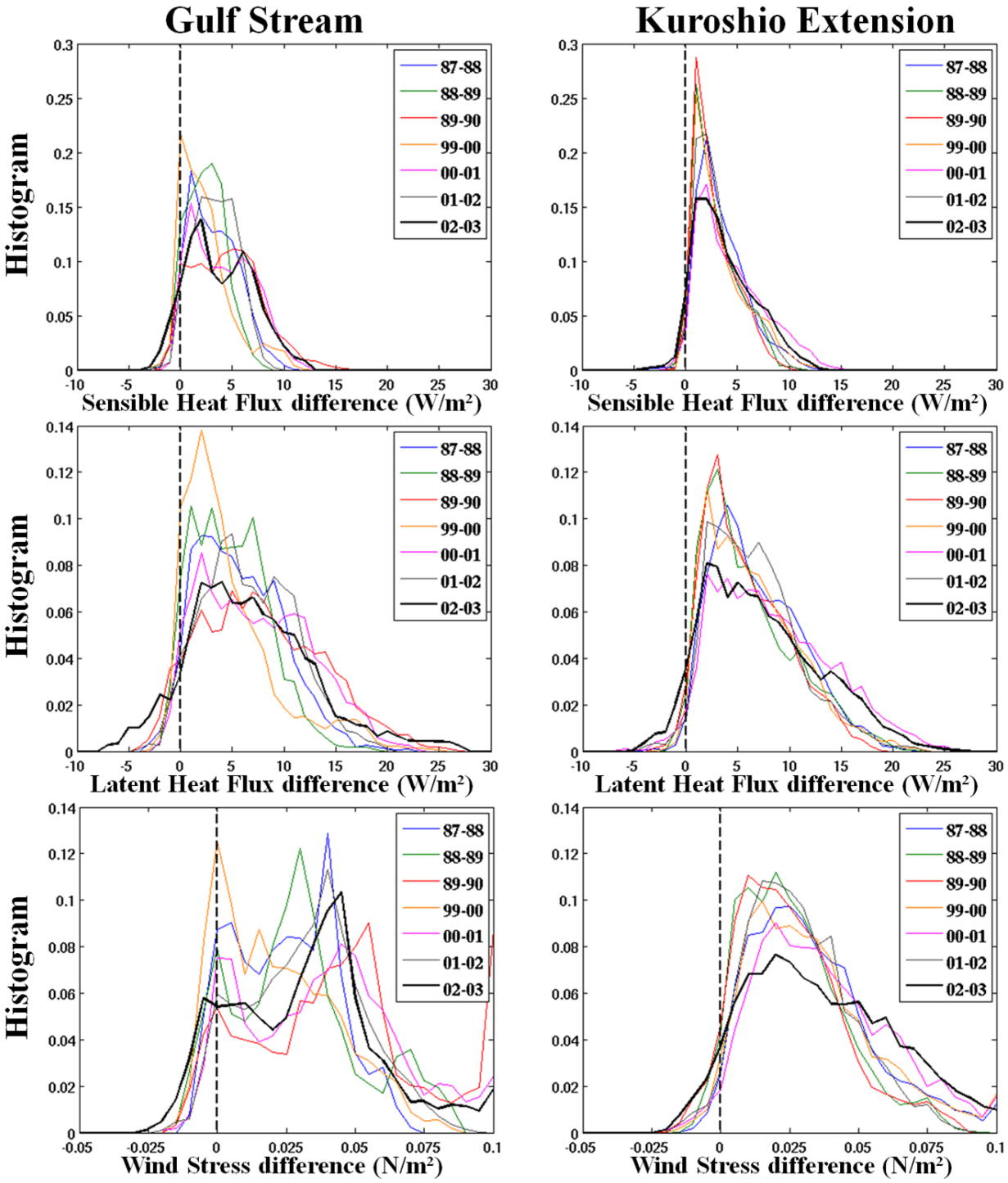

Figure 3.6: DJF seasonal histograms of SHF difference (top), LHF difference (middle), and wind stress difference (bottom) over the Gulf Stream (left) and Kuroshio Extension (right) for the years 1987–1988, 1988–1989, 1989–1990, 1999–2000, 2000–2001, 2001–2002.

3.3 Monthly turbulent flux differences

Monthly-averaged turbulent flux differences are more sensitive to the background synoptic-scale environment and demonstrate more spatial variability than the seasonal averages. While the monthly calendar is an expedient framework for organizing data, this approach may not be the best method for capturing synoptic-scale events. For example, a multi-day synoptic disturbance producing significant turbulent flux differences towards the end of a particular month and continuing into the beginning of the following month would be poorly represented in the time-average for either month [Lau, 1988]. Despite this shortfall, monthly averages provide further insight into the relationship between surface wind modifications near SST fronts and the resulting changes in surface turbulent fluxes. One advantage to using monthly averages is the ability to further resolve the annual cycle.

The months of January, April, July, and October 2003 were chosen as representative months since they all lie in the middle of their respective seasons (Fig. 3.7). Considerable turbulent flux differences exist over large sections of the Pacific and Atlantic Oceans during January 2003. Most notable is the enormous extent of turbulent flux differences greater than 10 W/m² and 0.05 N/m² located over a zonally elongated Kuroshio Extension (Fig. 3.7). Also, similar magnitudes in turbulent flux differences within the Gulf Stream system are located downstream, east of Newfoundland. By April, there is a drastic reduction in ∇SST-induced turbulent flux differences over the Gulf Stream and Kuroshio Extension with magnitudes mostly under 3 W/m² and 0.05 N/m². Only a small section of the Kuroshio Extension has wind stress differences greater than 0.05 N/m². In July, there are minimal turbulent flux differences over the Gulf Stream and Kuroshio Extension as the conditions that support these air-sea interactions cease. October has an expanded area of LHF differences greater than 5 W/m² and wind stress differences greater than 0.025 N/m² as more favorable conditions begin to return.

The monthly box-and-whisker plots highlight the annual cycle in surface turbulent flux differences. As expected, the months of December, January, and February have the largest magnitudes. For SHF, the median flux differences are around ~3 to 4 W/m² with the 75th percentiles approaching 7 W/m² (Fig. 3.8). The LHF differences are larger, as the median flux differences are near 7 W/m² and the 75th percentiles surpass 10 W/m². Wind stress differences with median values from 0.03 to 0.04 N/m² and the 75th percentiles closer to 0.05 N/m² are physically significant for oceanic forcing. These three months experience most of the

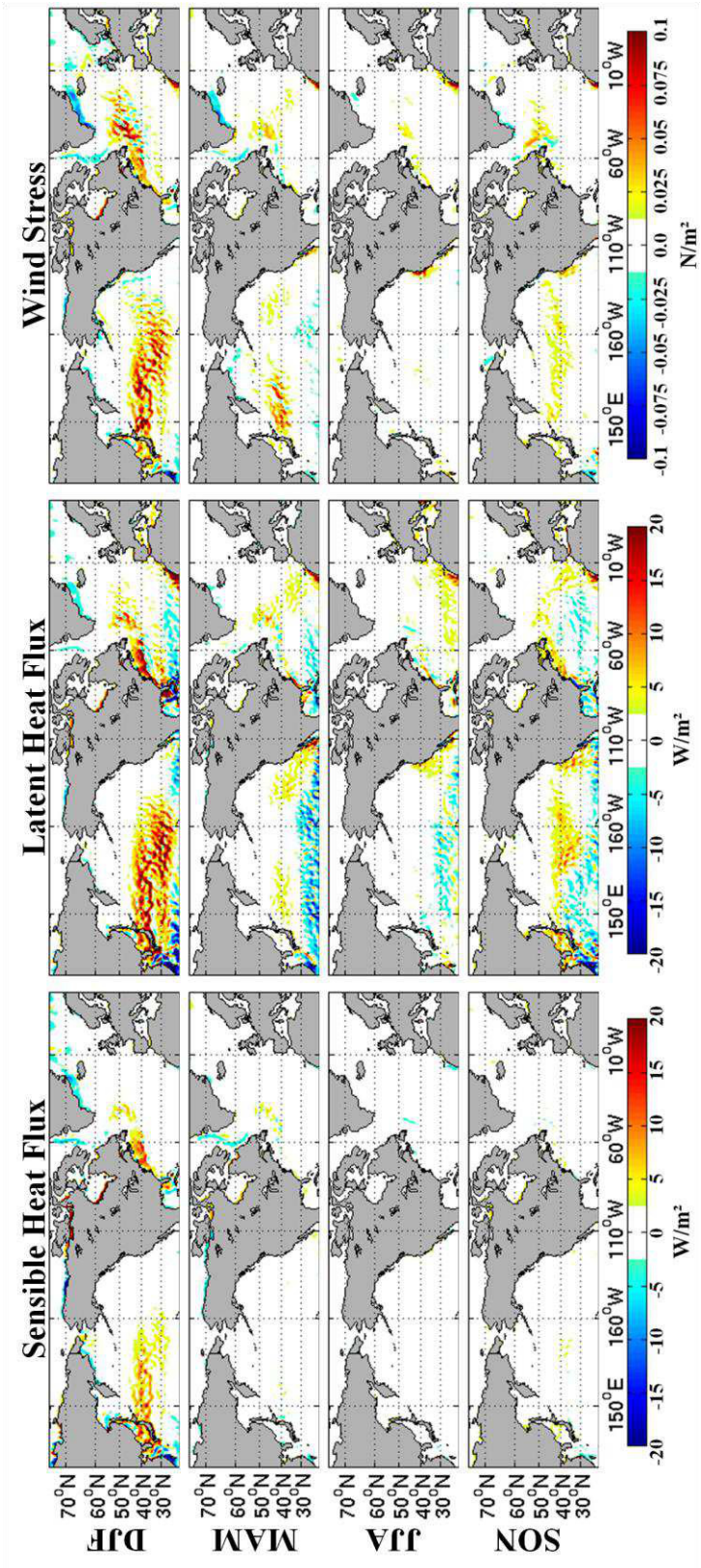

Figure 3.7: 2003 monthly average differences in SHF (left), LHF (middle), and wind stress (right) for January (top row), April (2nd row), July (3rd row), and October (bottom row).

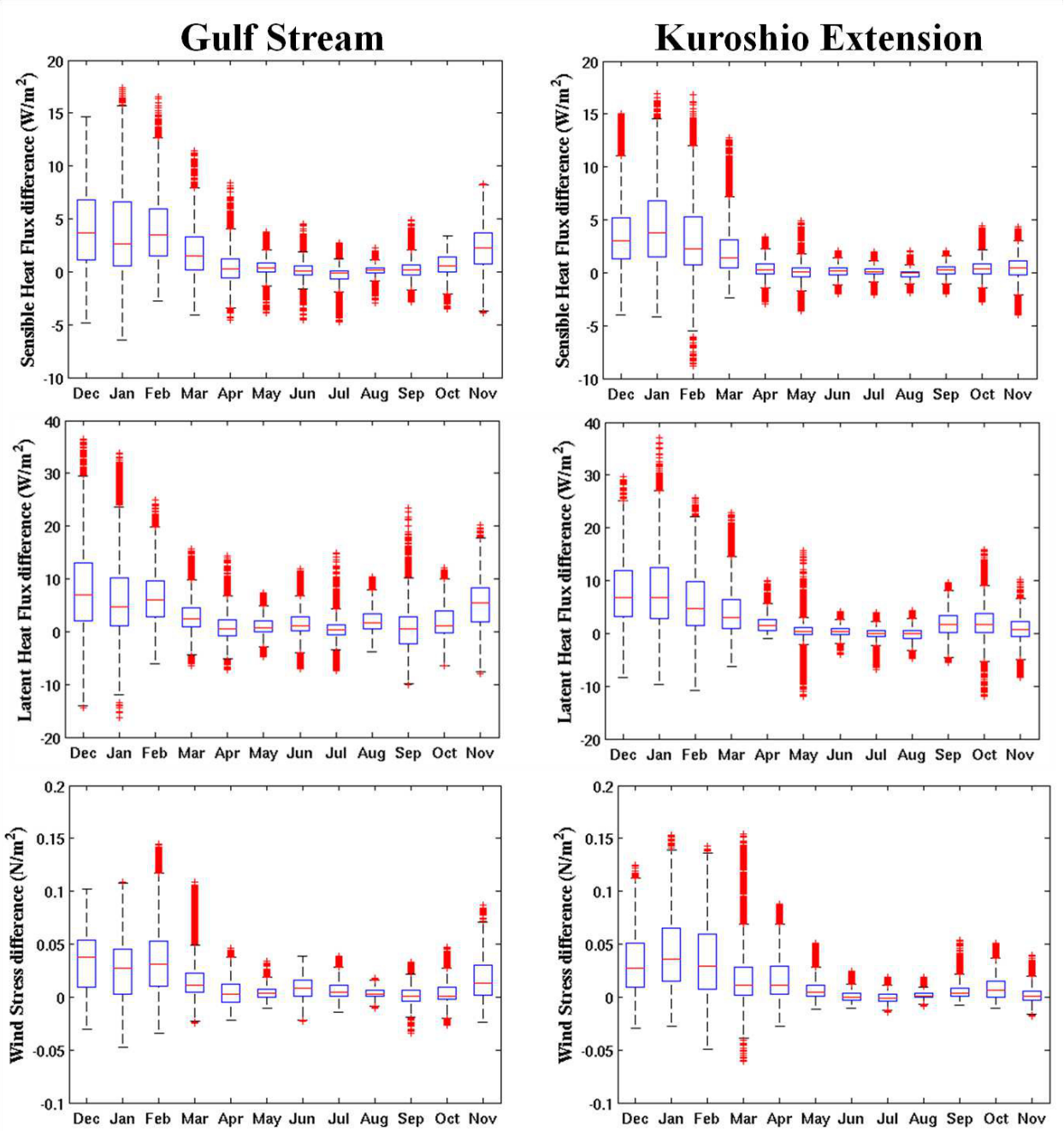

Figure 3.8: December 2002 – November 2003 monthly box-and-whisker plots of SHF difference (top), LHF difference (middle), and wind stress difference (bottom) over the Gulf Stream (left) and Kuroshio Extension (right).

∇SST-induced changes in surface turbulent fluxes, and they are the most important to consider when determining the impacts to the moisture and energy budgets. The spring and fall months are transitional periods where turbulent flux differences are small compared to winter but not

negligible. Generally, March has magnitudes greater than April and May as the synoptic-scale environment begins to change. The same holds true for November when compared to September and October. The median values for SHF, LHF, and wind stress differences over these transitional months are ~1 to 3 W/m², ~3 to 5 W/m², and ~0.01 to 0.02 N/m², respectively. Finally, the summer months of June, July, and August have very little turbulent flux difference and mark the minimum in the annual cycle.

3.4 Daily turbulent flux differences

Daily averaged turbulent flux differences have much higher variability as their magnitudes depend entirely on the current synoptic-scale environment. The daily averaged events provide a look at snapshots within the life cycle of individual synoptic-scale events that can impact the storm's evolution and properties within the oceanic mixed layer. High wind events over the Gulf Stream and Kuroshio Extension were hand selected for analysis by choosing one day from each of the seven DJF seasons. An ensemble of histograms and box-and-whisker plots were constructed (Figs. 3.9 and 3.10) from these daily averages. All histograms are unimodal with a slightly positive central peak and positive skewness (Fig. 3.9). The positive tails of turbulent flux histograms extend out to 40–80 W/m² for the heat fluxes and 0.2–0.5 N/m² for wind stress. Despite the same physical processes taking place over the Gulf Stream and Kuroshio Extension, the histogram shapes are slightly different between the two regions. The Gulf Stream heat flux histograms have a steeper central peak and the tails fall off rapidly. However, the Kuroshio Extension heat flux histograms have a flatter central peak with positive tails that gradually taper off. Also, more extreme heat flux differences occur over the Gulf Stream with values approaching 70–90 W/m²; a result not observed in the Kuroshio Extension daily histograms (Fig. 3.9). The histograms for wind stress have the opposite relationship, with a more gradual decay of the central peak for the Gulf Stream and a steep peak for the Kuroshio Extension. These differences between the two regions likely results from surface winds crossing the SST fronts at different angles since the Kuroshio Extension can be more zonally oriented than the Gulf Stream. Theoretically, this scenario would produce more extreme flux differences over the Gulf Stream since the crossing angle is closer to perpendicular.

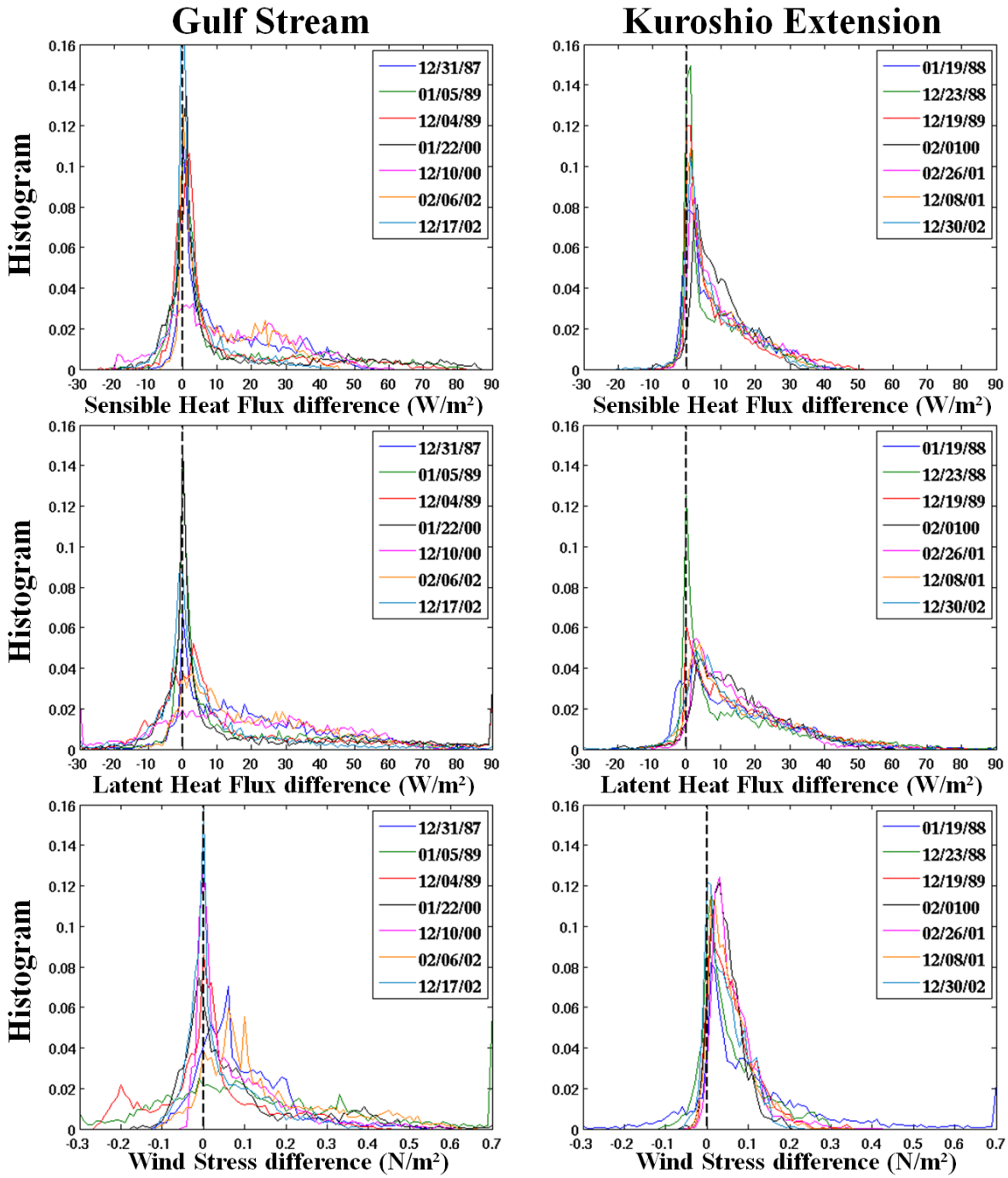

Figure 3.9: Daily histograms of SHF difference (top), LHF difference (middle), and wind stress difference (bottom) over the Gulf Stream (left) and Kuroshio Extension (right) during selected high wind events.

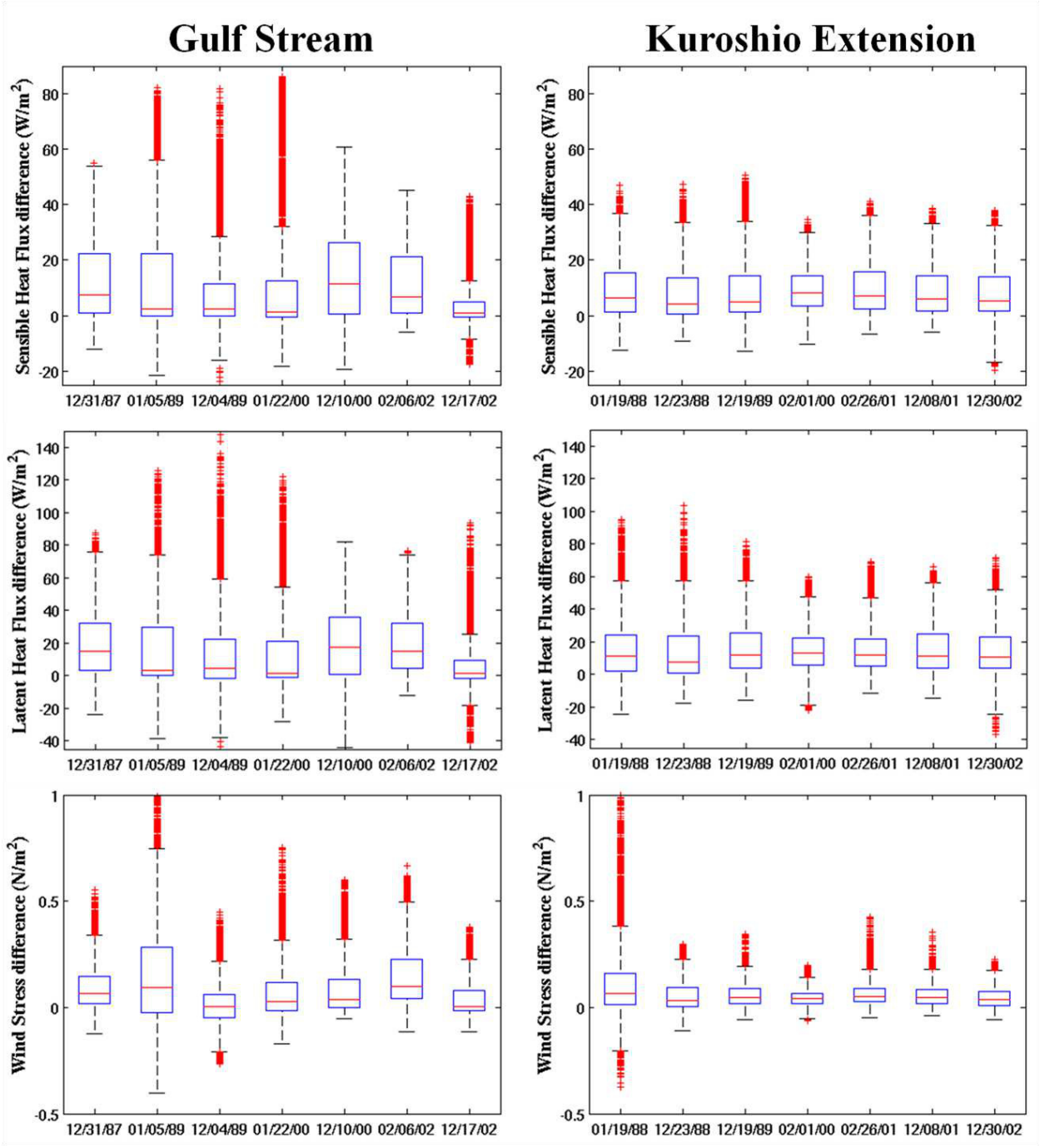

Figure 3.10: Daily box-and-whisker plots of SHF difference (top), LHF difference (middle), and wind stress difference (bottom) over the Gulf Stream (left) and Kuroshio Extension (right) during selected high wind events.

3.5 Discussion

Surface turbulent flux differences for December 2002 through November 2003 were averaged over seasonal, monthly, and daily time scales. The largest ∇SST-induced impacts to surface fluxes occur during the winter as high wind events are more frequent and the surface layer is typically more unstable. On seasonal and monthly time scales, heat flux differences during winter are typically 5 to 10 W/m². At smaller time scales, daily averaged heat flux differences during high wind events are 10 to 20 W/m². The histograms for the Gulf Stream and Kuroshio Extension have some interesting differences. Most notably, the Gulf Stream histograms have steeper central peaks and tails that extend out to more extreme values. The distinct features in the histograms between these two regions are likely due to regional differences in the distributions of near-surface stability and to dissimilarity between the Gulf Stream and Kuroshio Extension transport characteristics. A key difference between these two regions is the large scale sinking of dense surface water that occurs in the North Atlantic Ocean. As the northern extension of the Gulf Stream replenishes surface waters, the areas of large SST gradients can be displaced further north. Contrarily, the Kuroshio Extension is more zonally oriented and located further south. Therefore, the location and orientation of the largest SST gradients within the Gulf Stream and Kuroshio Extension likely influence the distributions of surface turbulent fluxes.

The seasonal dependence of surface turbulent flux differences results from two main factors. First, near-surface stability over the Gulf Stream and Kuroshio Extension is largely unstable during the winter as relatively colder air is present over warm SSTs (Fig. 3.11). Large surface instabilities allow higher momentum air from above to be more efficiently mixed downward, thereby increasing surface wind speeds and turbulent fluxes. Second, the magnitudes of these differences are dependent on the surface wind speed. In winter, surface winds tend to be stronger over the Gulf Stream and Kuroshio Extension regions as synoptic-scale frontal systems occur more frequently (Fig. 3.11). Summertime regimes are characterized by lighter wind speeds associated with the strengthening of the subtropical ridge. The magnitude of the SST gradient is also important; however, it changes on a much slower time scale. Therefore, surface turbulent flux differences due to the small-scale coupling between SSTs and wind speed is expected to be seasonally dependent.

The consistency in the Kuroshio Extension histograms among all DJF seasons (Fig. 3.6) is a surprising result because the background synoptic-scale environment plays a large role in

these physical processes. A significant source of turbulent flux differences occurs as relatively cool, dry air is advected across the SST front after the passage of midlatitude storm systems. The frequency, intensity, and path of synoptic-scale storm systems over the Gulf Stream and Kuroshio Extension can have considerable interannual variability during DJF and can be affected by large-scale teleconnections, such as El Niño Southern Oscillation (ENSO) and the North Pacific and North Atlantic Oscillations [Lau, 1988]. Specifically, ENSO is known to modify regional weather patterns across the globe. The Oceanic Niño Index (ONI) and ENSO phase are listed for each of the seven DJF seasons analyzed (Table 3.3). The ONI is determined by calculating a 3 month running mean of the Extended Reconstructed SST version 3b (ERSST.v3b) SST anomalies in the Niño 3.4 region (5°N - 5°S, 120° - 170°W) [Smith et al., 2008]. Interestingly, the two DJF seasons with the smallest differences in turbulent fluxes over the Gulf Stream are 1988–1989 and 1999–2000 (Fig. 3.6), strong La Niña years (Table 3.3). This observation does not extend to the Kuroshio Extension histograms. Also, there is no apparent connection between El Niño conditions and increased turbulent flux differences for the DJF seasons studied. To substantiate these observations further, separate analyses of strong La Niña DJF seasons and strong El Niño DJF seasons would be needed. The slight differences in the seven DJF histogram distributions are likely a result of this synoptic-scale variability. Therefore, the distributions of turbulent flux differences near SST fronts seem to not be overly sensitive to fluctuations in the large-scale environment during DJF.

Table 3.3: Oceanic Niño Index (ONI) and ENSO phase (shaded) for all DJF seasons analyzed.

DJF Season	DJF Niño 3.4 region SST Anomaly (°C)	ENSO Phase
1987–1988	0.8	El Niño
1988–1989	-1.7	La Niña
1989–1990	0.1	Neutral
1999–2000	-1.7	La Niña
2000–2001	-0.7	La Niña
2001–2002	-0.2	Neutral
2002–2003	1.1	El Niño

In addition, low-frequency changes in the surface transport characteristics of the Gulf Stream and Kuroshio Extension may impact turbulent flux differences for individual DJF seasons. The Kuroshio Extension is characterized by its large eastward surface transport and zonal penetration. Variability in the zonal-mean surface transport of the Kuroshio Extension is correlated to changes in its zonal-mean position and the strength of the southern recirculation gyre [Qiu et al., 1991]. A similar positive correlation between surface transport and zonal-mean position exists in the Gulf Stream system as well [Kelly, 1991]. As a result, there are two main states characterizing the Kuroshio Extension: an elongated and a contracted state. The elongated state has stronger eastward surface transport, greater zonal penetration, and an intense, zonally elongated southern recirculation gyre. Also, the zonal-mean Kuroshio Extension path is displaced to higher latitudes than its climatological mean position. In contrast, the contracted state has a weaker eastward surface transport, a smaller zonal penetration, a weaker southern recirculation gyre, and a more southerly zonal-mean path [Qiu, 2000]. Therefore, the meridional position and zonal extent of both the Gulf Stream and Kuroshio Extension can affect the magnitude and location of maximum ∇SST-related turbulent flux differences. Since no substantial changes in turbulent flux differences were observed in the six DJF seasons analyzed, it is likely that impacts from the low-frequency variability of the Gulf Stream and Kuroshio Extension were not captured, or that the changes in the distribution of winds and/or stratification roughly compensate the effects of changes in the SST gradients (Fig. 3.11). Such compensation was found in bulk stresses estimated from research vessel observations [May and Bourassa, 2011]. Alternatively, changes in the crossing angle of the winds over the SST gradients could compensate for changes in the distribution of SST gradients. Furthermore, DJF seasonal analyses spanning multiple decades would be needed to assess whether an interannual or decadal pattern in ∇SST-induced turbulent flux differences is present due to low-frequency variability in atmospheric circulations and western boundary currents.

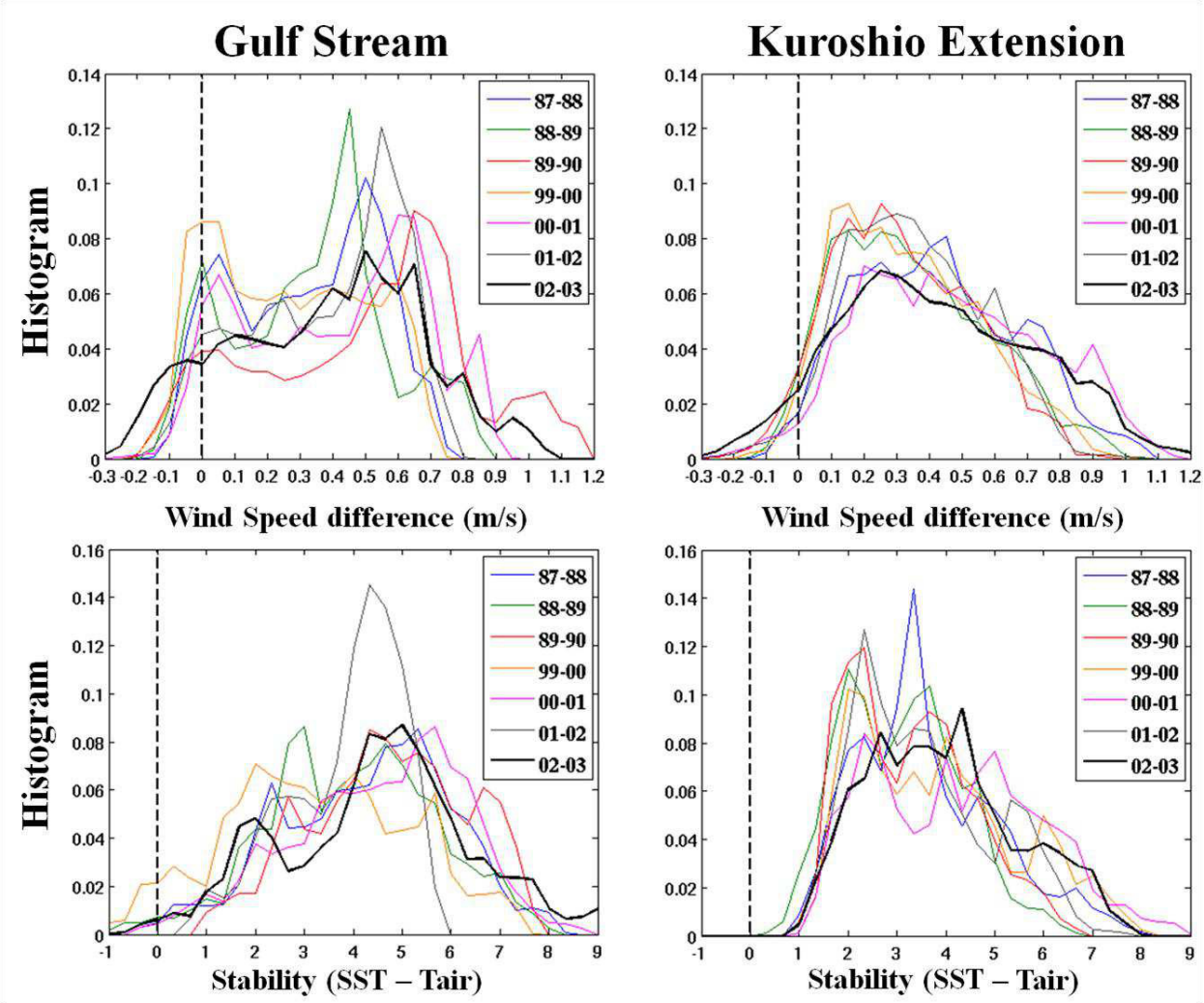

Figure 3.11: DJF seasonal histograms of wind speed difference (top) and near-surface stability (bottom) over the Gulf Stream (left) and Kuroshio Extension (right) for the years 1987–1988, 1988–1989, 1989–1990, 1999–2000, 2000–2001, 2001–2002.

CHAPTER FOUR

CONCLUSIONS

Western boundary currents such as the Gulf Stream and Kuroshio Extension have significant climatological impacts on large-scale oceanic and atmospheric circulations. Warm, subtropical water is transported poleward in these regions, creating large SST gradients (~ 2.2K/100 km) on spatial scales of ~100–200 km that modify small-scale (< 1000 km) surface winds. A positive correlation between SSTs and wind stress perturbation exists in these regions, leading to enhanced surface winds and fluxes on the warm side of the SST front and suppressed surface winds and fluxes on the cold side. These ∇SST-induced changes to the surface winds are poorly modeled in NWP, climate models, and gridded reanalyses, resulting in an underestimation of the small-scale wind variability. As a result, these errors are propagated in bulk formula estimates of surface turbulent fluxes.

Surface turbulent fluxes in gridded products (e.g., reanalyses) have large biases over the Gulf Stream and Kuroshio Extension due to the small-scale coupling that exists between SSTs and surface winds. These processes are not well represented in reanalysis data sets at this time. The greatest ∇SST-induced impacts occur during winter as the climatological synoptic-scale environment supports more baroclinic activity and strong SST gradients persist, leading to large surface instabilities (SST – air temperature) that enhance turbulent fluxes out of the ocean. The favorable conditions that drive these strong air-sea interactions over the Gulf Stream and Kuroshio Extension subside during the spring, are mostly absent over summer, and increase in the fall.

Surface wind perturbations and enhanced turbulent fluxes near SST gradients impact the ocean and atmosphere across varying spatial and temporal scales. Mesoscale and synoptic-scale atmospheric processes such as coastal frontogenesis, low-level jet formation, low-level cloud and rainband generation, and the intensification of midlatitude frontal systems are all affected by large turbulent heat fluxes. Additionally, surface turbulent flux differences influence oceanic mixed layer properties and localized ocean circulations. On larger scales, diabatic heating from surface heat fluxes over the Gulf Stream and Kuroshio Extension helps maintain climatological atmospheric circulations in the midlatitudes. Also, multi-decadal variability in upper ocean heat content is sensitive to heat flux differences as small as several tenths of 1 W/m² [Levitus et al.,

2005]. To assess the impact that ∇SST-induced changes to surface turbulent fluxes have on these atmospheric and oceanic processes, bulk formula fluxes are averaged over seasonal, monthly, and daily time scales from December 2002 through November 2003. To further quantify ∇SST impacts during winter, six additional DJF seasons from 1987–1990 and 1999–2002 were analyzed. DJF seasonally averaged differences in SHF, LHF, and wind stress for all seven DJF seasons studied range from 2.4 to 4.5 W/m², 4.7 to 8.4 W/m², and 0.022 to 0.045 N/m², respectively. These considerable seasonal flux differences cover an expansive area near the Gulf Stream and Kuroshio Extension and likely influence regional atmospheric and oceanic processes nearby. As the averaging time scale decreases there is more spatial variability in the largest turbulent flux differences since synoptic-scale environmental factors such as storm path and intensity can be highly variable. Daily averaged turbulent flux differences during wintertime high wind events have typical values ranging from 10 to 20 W/m² and 0.05 to 0.15 N/m² for heat and momentum fluxes, respectively. Turbulent flux differences over the course of a single synoptic wind event can impact midlatitude storm evolution.

The ability to simulate air-sea interactions over strong SST fronts degrades with decreasing spatial resolution and results in an underestimation of the covariability in surface wind and SST, both of which are important terms in bulk formula estimates of air-sea fluxes. As a consequence, appreciable regional errors in the energy and moisture budgets likely exist in climate models and reanalysis data sets due to their inability to effectively resolve these surface processes. A better representation of the small scale coupling between SSTs and winds near SST gradients in boundary layer parameterizations should improve NWPs and climate models. However, at this time there are very few boundary layer models that are able to capture the small-scale wind variability seen in satellite observations [Song et al., 2009]. In addition, the inclusion of denser observations over the Gulf Stream and Kuroshio Extension are needed to accurately measure fluxes in these regions. Alternatively, the ability to parameterize the linear relationships between SST perturbations and wind stress perturbations near strong SST gradients would minimize some of these deficiencies. As these advancements are made, modeled surface turbulent fluxes will lead to a more accurate representation of regional energy, moisture, and momentum budgets.

REFERENCES

Beljaars, A.C. M., and A. A. M. Holtslag, (1991), Flux parameterization over land surfaces for atmospheric models, *J. Appl. Meteorol*., *30*, 327-341.

Benoit, R., (1977), On the integral of the surface layer profile-gradient functions, *J. Appl. Meteorol*., *16*, 859-860.

Bourassa, M. A., D. G. Vincent, and W. L. Wood, (1999), A flux parameterization including the effects of capillary waves and sea state, *J. Atmos. Sci.*, *56*, 1123-1139.

Bourassa, M. A., (2006), Satellite-based observations of surface turbulent stress during severe weather, *Atmosphere - Ocean Interactions*, *2*, 35-52.

Brown, R. A., (1974), Analytical methods in planetary-layer modeling, Adam Hilger Ltd., London.

Brown, R. A., (1978), Similarity parameters from first-order closure and data, *Bound.-Layer Meteor.*, *14*, 381-396.

Brown, R. A., and W. T. Liu, (1982), An operational large-scale marine planetary boundary layer model. *Bound.-Layer Meteor.*, *21*, 261-269.

Chelton, D. B., S. K. Esbensen, M. G. Schlax, N. Thum, M. H. Freilich, F. J. Wentz, C. L. Gentemann, M. J. McPhaden, and P. S. Schopf, (2001), Observations of coupling between surface wind stress and sea surface temperature in the eastern tropical Pacific, *J. Climate*, *14*, 1479-1498.

Chelton, D. B., M. G. Schlax, M. H. Freilich, and R. F. Milliff, (2004), Satellite measurements reveal persistent small-scale features in ocean winds, *Science*, *303*, 978-983.

Chelton, D. B., (2005), The impact of SST specification on ECMWF surface wind stress fields in the eastern tropical Pacific, *J. Climate*, *18*, 530-550.

Chelton, D. B., M. G. Schlax, and R. M. Samelson, (2007), Summertime coupling between sea surface temperature and wind stress in the California Current System, *J. Phys. Ocean.*, *37*, 495-517.

Clayson, C. A., C. W. Fairall, and J. A. Curry, (1996), Evaluation of turbulent fluxes at the ocean surface using surface renewal theory, *J. Geophys. Res.*, *101*, 28,503-28,513.

Dee, D. P., S. M. Uppala, A. J. Simmons, P. Berrisford, P. Poli, S. Kobayashi, U. Andrae, M. A. Balmaseda, G. Balsamo, P. Bauer, P. Bechtold, A. C. M. Beljaars, L. van de Berg, J. Bidlot, N. Bormann, C. Delsol, R. Dragani, M. Fuentes, A. J. Geer, L. Haimberger, S. B. Healy, H. Hersbach, E. V. Hólm, L. Isaksen, P. Kållberg, M. Köhler, M. Matricardi, A. P. McNally, B. M. Monge-Sanz, J.-J. Morcrette, B.-K. Park, C. Peubey, P. de Rosnay, C. a Tavolato, J.-N. Thépaut, and F. Vitart, (2011), The ERA-Interim reanalysis: configuration and performance of the data assimilation system. *Q.J.R. Meteorol. Soc*., *137*, 553–597.

Hogg, A. McC., W. K. Dewar, P. Berloff, S. Kravtsov, and D. K. Hutchinson, (2009), The effects of mesoscale ocean-atmosphere coupling on the large-scale ocean circulation, *J. Climate, 22*, 4066-4082.

Josey, S. A., E. C. Kent, and P. K. Taylor, (1999), New insights into the ocean heat budget closure problem from analysis of the SOC air-sea flux climatology, *J. Climate*, *12*, 2856-2880.

Kelly, K. A., (1991), The meandering Gulf Stream as seen by the Geosat altimeter: Surface transport, position, and velocity variance from 73° to 46°W, *J. Geophys. Res.*, *96*, 721-738.

Lau, N.-C., (1988), Variability of the observed midlatitude storm tracks in relation to low-frequency changes in the circulation pattern, *J. Atmos. Sci.*, *45*, 2718-2743.

Levitus, S., J. I. Antonov, and T. Boyer, (2005), Warming of the World Ocean, 1955–2003, *Geophys. Res. Lett., 32***,** L02604.

Lindzen, R. S., and S. Nigam, (1987), On the role of sea surface temperature gradients in forcing low-level winds and convergence in the tropics, *J. Atmos. Sci., 44***,** 2418–2436.

Liu, W. T., K. B. Katsaros, and J. A. Businger, (1979), Parameterization of air-sea exchanges of heat and water vapor including the molecular constraints at the interface, *J. Atmos. Sci.*, *36*, 1722-1735.

Maloney, E. D., and D. B. Chelton, (2006), An assessment of the sea surface temperature influence on surface wind stress in numerical weather prediction and climate models, *J. Climate*, *19*, 2743-2762.

May, J. C., and M. A. Bourassa, (2011), Quantifying variance due to temporal and spatial difference between ship and satellite winds, *J. Geophys. Res.*, 116, C08013.

Milliff, R. F., J. Morzel, D. B. Chelton, and M. H. Freilich, (2004), Wind stress curl and wind stress divergence biases from rain effects on QSCAT surface wind retrievals, *J. Atmos. Oceanic Technol.*, *21*, 1216-1231.

Minobe, S., A. Kuwano-Yoshida, N. Komori, S.-P. Xie, and R. J. Small, (2008), Influence of the Gulf Stream on the troposphere, *Nature*, *452*, 206-210.

Nonaka, M.,and S.-P. Xie, (2003), Covariations of sea surface temperature and wind over the Kuroshio and its extension: Evidence for ocean-to-atmosphere feedback, *J. Climate*, *16*, 1404–1413.

O'Neill, L. W., D. B. Chelton, and S. K. Esbensen, (2003), Observations of SST-induced perturbations of the wind stress field over the Southern Ocean on seasonal timescales, *J. Climate*, *16*, 2340-2354.

O'Neill, L. W., D. B. Chelton, and S. K. Esbensen, (2005), High-resolution satellite measurements of the atmospheric boundary layer response to SST variations along the Agulhas return current, *J. Climate*, *18*, 2706-2723.

O'Neill, L. W., D. B. Chelton, and S. K. Esbensen, (2010), The effects of SST-induced surface wind speed and direction gradients on midlatitude surface vorticity and divergence, *J. Climate*, *23*, 255-281.

O'Neill, L. W., (2012), Wind speed and stability effects on coupling between surface wind stress and SST observed from buoys and satellite, *J. Climate*, *25*, 1544-1569.

Qiu, B., K. A. Kelly, and T. M. Joyce, (1991), Mean flow and variability in the Kuroshio Extension from Geosat altimetry data, *J. Geophys. Res.*, *96*, 18,491-18,507.

Qiu, B., (2000), Interannual variability of the Kuroshio Extension system and its impact on the wintertime SST field, *J. Phys. Ocean*, *30*, 1486-1502.

Reynolds, R. W., T. M. Smith, C. Liu, D. B. Chelton, K. S. Casey, and M. G. Schlax, (2007), Daily high-resolution-blended analyses for sea surface temperature, *J. Climate*, *20*, 5473-5496.

Rouault, M., C. J. C. Reason, J. R. E. Lutjeharms, A. C. M. Beljaars, (2003), Underestimation of latent and sensible heat fluxes above the Agulhas Current in NCEP and ECMWF analyses, *J. Climate*, *16*, 776-782.

Small, R. J., S. P. deSzoeke, S.-P. Xie, L. O'Neill, H. Seo, Q. Song, P. Cornillon, M. Spall, and S. Minobe, (2008), Air-sea interaction over ocean fronts and eddies, *Dyn. Atmos. Oceans*, *45*, 274-319.

Smith, T. M., R. W. Reynolds, T. C. Peterson, and J. Lawrimore, (2008), Improvements to NOAA's historical merged land-ocean surface temperature analysis (1880–2006), *J. Climate*, *21*, 2283-2296.

Song, Q., P. Cornillon, and T. Hara, (2006), Surface wind response to oceanic fronts. *J. Geophys. Res.*, *111*, C12006.

Song, Q., D. B. Chelton, S. K. Esbensen, N. Thum, and L. W. O'Neill, (2009), Coupling between sea surface temperature and low-level winds in mesoscale numerical models, *J. Climate*, *22*, 146-164.

Wallace, J. M., T. P. Mitchell, and C. Deser, (1989), The influence of sea surface temperature on surface wind in the eastern equatorial Pacific: Seasonal and interannual variability, *J. Climate, 2*, 1492–1499.

Wikle, C. K., R. F. Milliff, and W. G. Large, (1999), Surface wind variability on spatial scales from 1 to 1000 km observed during TOGA COARE, *J. Atmos. Sci.*, *56*, 2222-2231.

Xue, H., Z. Pan, and J.M. Bane, (2000), A coupled atmosphere–ocean study of air–sea interactions during a cold air outbreak over the Gulf Stream, *Mon.Wea. Rev.*, *128*, 973-996.

Zheng, Y., M. A. Bourassa, and P. J. Hughes, (2013), Influences of sea surface temperature gradients and surface roughness changes on the motion of surface oil: A simple idealized study, *J. Appl. Meteor. Clim*., *52*, 1561-1575.

BIOGRAPHICAL SKETCH

I was raised in Jacksonville, Florida by my parents, Wade and Connie Steffen. I have a sister, Rachel, who is finishing her M.S. in Occupational Therapy at the University of Florida. Growing up in Florida, hurricanes were of particular interest to me. My curiosity in tropical meteorology was strengthened when four hurricanes made landfall in Florida during the 2004 hurricane season. I attended Stanton College Preparatory School and completed the International Baccalaureate program in 2006. I continued my education at the University of Florida, earning a B.A. in Physics and a minor in Geography. After taking a year off from school to teach, I entered the M.S. Meteorology program at Florida State University in the Department of Earth, Ocean, and Atmospheric Sciences. Beyond my academic interests, I also enjoy playing sports, camping, traveling, and being outdoors with my Golden Retriever, Daisy.